American Mineralogist, Volume 71, pages 569–588, 1986

Mineralogy and radiation effects of microlite from the Harding pegmatite, Taos County, New Mexico

G. R. LUMPKIN, B. C. CHAKOUMAKOS, AND R. C. EWING
Department of Geology, University of New Mexico, Albuquerque, New Mexico 87131

ABSTRACT

Microlite, ranging from crystalline to metamict, is a principal accessory in several lithologic units of the Harding pegmatite, Taos County, New Mexico. From the sequence of lithologic units within the pegmatite, crystallization of microlite from the pegmatite magma is inferred to have begun relatively late, after the formation of the beryl and quartz zones, and continued throughout the formation of the core zones and subsolidus replacement units. Over 200 chemical analyses of microlite determined by electron microprobe are reported, and they are consistent with the accepted structural formula, $A_{2-m}B_2X_6Y_{1-n}\cdot pH_2O$, where principally A = Ca, Na, U, Mn; B = Ta, Nb, Ti; X = O; and Y = F, OH, O. General features of microlite crystal chemistry identified include (1) a positive correlation between A-site vacancies and the maximum Y-site vacancies, (2) a positive correlation between Na and F, and (3) a negative correlation between U and F. The latter is consistent with the interpretation that U at the A site in the pyrochlore structure is analogous to the uranyl group, UO_2^{2+}, requiring O in place of F at the Y site. Microlite compositions from four of five lithologic units examined are chemically distinct in terms of linear combinations of the variables U, Fe, Ti, Bi, Ca, Ce, Pb, F, Mn, Ba, Sb, Th, Ta, and Na. The cleavelandite-unit microlites, the exception, not surprisingly have chemistries like those of the quartz–lath spodumene zone, which the cleavelandite unit in part has replaced. The earliest-formed microlites from the quartz–lath spodumene zone have the highest Ta, Na, and F and are low in U and Mn. In contrast, microlites from the later microcline-spodumene zone and the replacement units are generally higher in Ti, Mn, and U and lower in F and Na. Chemical changes ascribed to primary hydrothermal alteration from residual pegmatitic fluids include increases in Ca, Mn, and Ti and an overall loss of A-site cations. Alteration effects and chemical zoning within crystals, analyzed in terms of simple end members, identifies the following principal substitution schemes: ${}^{B}Nb \rightarrow {}^{B}Ta$, ${}^{B}Ta \rightarrow {}^{B}Nb$, ${}^{A}Ca^{Y}O \rightarrow {}^{A}Na^{Y}F$ and ${}^{A}\square^{Y}\square \rightarrow {}^{A}Na^{Y}F$ for core-to-rim zoning in crystals and ${}^{A}Ca^{Y}O \rightarrow {}^{A}Na^{Y}F$ and ${}^{A}Ca^{Y}O \rightarrow {}^{A}\square^{Y}\square$ for primary alteration. Secondary (weathering) alteration results in decreases in Na, Ca, and F and increases in H_2O.

The effects of alpha-recoil damage due to the decay of constituent U have been examined. Because of the wide variation in U content (0.1–10 wt% UO_3), the microlites exhibit the full range of structural periodicity from completely crystalline (<1 dpa), partially crystalline (up to 10–20 dpa) to completely X-ray and electron diffraction amorphous (>20 dpa). Based on X-ray and electron diffraction analysis, the progressive structural modification of microlite with increasing alpha dose involves (1) formation of isolated defect aggregates (i.e., individual alpha-recoil tracks) up through doses of 10^{14} alphas/mg with no detectable effect on the materials's ability to diffract X-rays or electrons, (2) continued damage and overlap of these defect aggregates yielding coexisting regions of amorphous and crystalline domains at 10^{15} to 10^{16} alphas/mg, and (3) complete amorphization at doses greater than 10^{17} alphas/mg.

INTRODUCTION

Minerals of the pyrochlore group (*Fd*3*m*, Z = 8) have the general formula $A_{2-m}B_2X_6Y_{1-n}\cdot pH_2O$, where A = Na, Ca, U, Pb, Sr, Th, REE, Bi, Sn^{2+}, Ba, Mn, Fe^{2+}; B = Ta, Nb, Ti, Zr, Fe^{3+}, Sn^{4+}, W; X = O; and Y = O, OH, F. Hogarth (1977) defined the microlite subgroup to have Ta ≥ Nb and Nb + Ta > 2Ti. Most natural compositions have <10 mol% Ti and <25 mol% Nb (Lumpkin and Ewing, 1985). Except for a single report of microlite occurring in a granite (Sitnin and Bykova, 1962), most microlites are found in granitic pegmatites of the rare-element class (Černý, 1982; Černý and Burt, 1984). The typical accessory minerals associated with microlite include zircon, stibiotantalite, bismutotantalite, columbite-

0003–004X/86/0304–0569$02.00

tantalite, rynersonite, wodginite, and simpsonite (Von Knorring and Fadipe, 1981; Foord, 1982).

Microlite was first described from the Harding pegmatite by Hirschi (1931), and during the period 1942–1947 over 11 tons were produced by hand-mining methods (Jahns and Ewing, 1976, 1977). The microlite concentrates averaged 68 wt% Ta_2O_5 and 7 wt% Nb_2O_5. The first complete chemical analyses correlated the change from light to dark color in five microlites with decreasing Ta/Nb ratio and increasing OH/F ratio and the U, Ti, and Mn content (Jahns and Ewing, 1976). Partial electron-microprobe analyses (Suchomel, 1976) confirmed these trends for Ta/Nb, Ti, and Mn. Suchomel did not analyze for F and U, so the analyses do not conform to the pyrochlore structural formula (Chakoumakos, 1978).

Microlites are stable from ca. 500°C and 5 kbar down to ambient, near-surface conditions and can accommodate a variety of rare elements as a function *T, P,* and melt/fluid composition. Microlites from African localities were broadly classified as primary, secondary, and uraniferous types by Von Knorring and Fadipe (1981). They suggested that with time, microlites generally show decreasing amounts of Ta, Ca, and F with increasing concentrations of Ti, U, Sb, Bi, Pb, and H_2O. However, little is known about chemical variations in microlites within individual pegmatites (cf., Mihálik, 1967; Foord, 1976). The abundance of microlite in several lithologic units of the Harding pegmatite provides an excellent opportunity to examine these chemical trends.

Prior to this work, Suchomel (1976) noted higher Nb_2O_5 and lower Ta_2O_5 contents in microlites from the microcline–spodumene zone ("spotted rock") relative to those from other units. Chakoumakos (1978) made an extensive petrographic and X-ray diffraction study of 30 located samples, three high-grade ore samples, and two analyzed samples. No relationship between degree of crystallinity and lithologic unit was noted, implying that U does not vary systematically within the pegmatite. Most of Chakoumakos' samples have been used in this study, along with additional specimens donated by Arthur Montgomery. The purpose of this paper is threefold: (1) to discuss general features of microlite crystal chemistry, (2) to examine relationships between composition and lithologic unit using statistical analysis, and (3) to describe radiation effects in microlites.

Location and general geology

The Harding pegmatite is located in the Picuris Range 10 km east of Dixon and 30 km southwest of Taos in sec. 29, T23N, R11E. The pegmatite lies within Precambrian rocks of the Vadito Group. The main dike is about 370 m long and up to 80 m wide in outcrop. The body is roughly tabular in shape with a maximum thickness of 25 m and an average plunge of 10°S (Jahns and Ewing, 1976, 1977). Exposures occur primarily along the boundary between amphibolite (hanging wall) on the south and pelitic schists (footwall) on the north (Long, 1974; Jahns and Ewing, 1976). Bedding (S_0) and transposition layering (S_0/S_1) trend N8°E in Vadito rocks north of the pegmatite. The primary foliation is slaty cleavage or schistosity (S_2) which trends N10°W and intersects bedding at a low angle (Holcombe and Callender, 1982). The pegmatite truncates S_0/S_1 and S_2 and must postdate F_1 and F_2 folding.

Several types of granitic rocks are present in the area. On the basis of field evidence and limited radiometric dating, Long (1974) considered the Harding and other pegmatites to be late in the history of granitic magmatism. He suggested a separate magmatic event for the pegmatites 100 m.y. later than the youngest (unfoliated) granite and as much as 300–400 m.y. later than the oldest (foliated) granitic rocks. Aldrich et al. (1958) determined K-Ar and Rb-Sr ages of 1260 m.y. for lepidolite from the Harding mine. Recent Rb-Sr ages of 1336 ± 73 for the "spotted rock" core unit, 1264 ± 128 for rose muscovite, and 1246 ± 40 m.y. for lepidolite were determined by Register (in Brookins et al., 1979).

Internal zoning and replacement units

The main pegmatite dike is characterized by an asymmetric sequence of lithologic units from top to bottom. These consist of six primary zones and two replacement units. The following description has been condensed from Jahns and Ewing (1976, 1977), Suchomel (1976), Chakoumakos (1978), and Norton (1983).

The hanging-wall portion of the pegmatite consists of three primary zones. The continuous *beryl zone* includes a thin, fine-grained border rind and coarser-grained wall zone composed of quartz, albite, and muscovite. Common accessory minerals are beryl, microcline, apatite, and columbite-tantalite. Below this is the *quartz zone,* a fairly continuous unit of massive quartz with accessory muscovite, microcline, and albite. The quartz zone is underlain by a spectacular *quartz–lath spodumene zone* characterized by spodumene crystals up to 2 m in length (see Fig. 6, Jahns and Ewing, 1976). Microlite, beryl, apatite, microcline, and lepidolite are common accessory minerals near the base of the discontinuous zone. The core of the pegmatite in the western thick end is dominated by the *microcline-spodumene zone,* otherwise known as "spotted rock." Microcline, spodumene, and quartz are the major minerals with minor amounts of apatite, albite, microlite, and columbite-tantalite. Fine-grained lepidolite and Li-bearing muscovite commonly replace microcline and spodumene. Locally, the unit grades into nearly pure masses of lepidolite. Two primary zones occur beneath the microcline-spodumene zone in the footwall portion of the pegmatite. The *perthite zone* is a discontinuous unit of blocky, perthitic microcline with minor quartz and albite. Beneath this is the *aplite zone,* composed of fine-grained albite and quartz with accessory beryl, apatite, and columbite-tantalite.

The primary zones have been replaced to varying degrees by two units. The *cleavelandite unit* is composed of platy albite, quartz, and minor muscovite. It occurs pri-

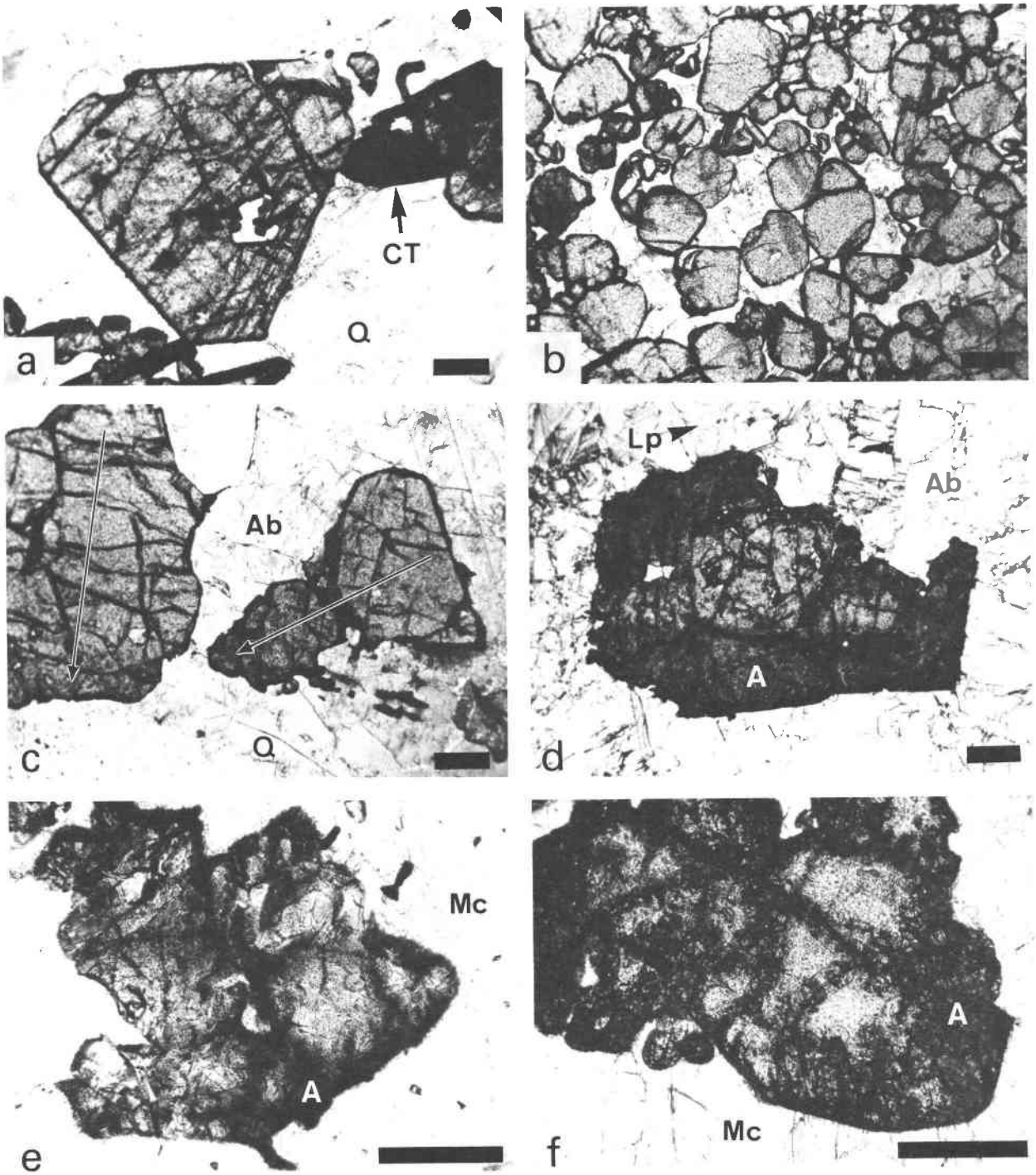

Fig. 1. Photomicrographs of microlite from the quartz–lath spodumene zone (a, b, c), cleavelandite replacement unit (d), and microcline-spodumene zone ("spotted rock") (e, f). Scale bars = 0.3 mm (a) Euhedral microlite (270) and columbite-tantalite (CT) in quartz (Q). (b) A cluster of subhedral microlite crystals (271) typical of high-grade ore. (c) Microlite in cleavelandite (Ab) pseudomorphic after spodumene. Crystals are zoned (arrows) toward the quartz interface. (d) An altered (A) microlite (P05.1) from a cleavelandite mass in the beryl zone. Matrix minerals are cleavelandite and lepidolite (Lp). (e) Anhedral microlite (P15.1) showing hydrothermal alteration along grain boundaries and fractures. Matrix mineral is microcline (Mc). (f) Altered and microfractured microlite (P17.1) in a microcline matrix. Unaltered areas of some grains are Pb-rich (see text).

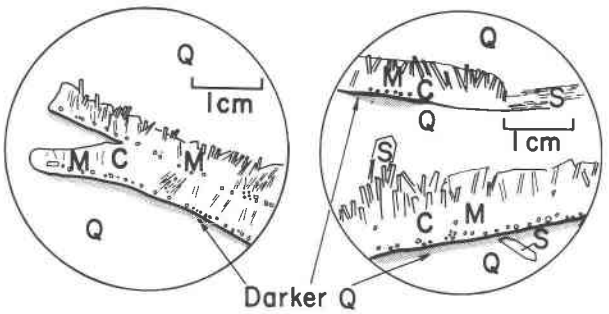

Fig. 2. Schematic cross sections of cleavelandite (C) replacements along possible pre-existing spodumene (S) laths. The matrix is pale smoky quartz (Q), which is dark smoky color (darker Q) adjacent to microlite (M) crystals segregated along the base of each "pseudomorph." The photomicrograph in Fig. 1c is an enlarged detail of the microlite. Sketches are from hand samples P11.3 (Chakoumakos, 1978).

marily in the core of the pegmatite, but also is found as scattered masses in the beryl zone (Chakoumakos, 1978). The *rose muscovite–cleavelandite unit* mainly replaced parts of the quartz–lath spodumene zone (Heinrich and Levinson, 1953).

Microlite petrography

The major occurrence of microlite is within the quartz–lath spodumene and microcline-spodumene ("spotted rock") zones. It is rare in the quartz zone where it occurs as honey-brown, microcrystalline aggregates along grain boundaries of accessory apatite (Suchomel, 1976). Microlite occurs with columbite-tantalite in the quartz–lath spodumene zone as euhedral to subhedral crystals (0.1–5 mm) poikilitically enclosed by quartz (Fig. 1a). The quartz fills interstices between interlocking spodumene laths. Microlite crystals tend to form dense aggregates (Fig. 1b) which provided most of the high-grade Ta-Nb ore. Colors range from pink, colorless, and pale green to shades of yellow and brown. Some crystals are zoned with light cores and dark rims. Lepidolite pods occurring near the base of the unit contain abundant, euhedral to subhedral, yellow microlite crystals (Montgomery, 1950).

In the microcline-spodumene zone, microlite is found as disseminated, euhedral to anhedral crystals enclosed in coarse-grained microcline (Figs. 1e, 1f). The color is dark brown to black. Most grains are 1.0 to 5.0 mm in size. Associated minerals include columbite-tantalite, hafnian zircon, and lepidolite. The Ta-Nb minerals average 0.15% in the microcline-spodumene zone, enough to consider this as low-grade ore (Jahns and Ewing, 1976, 1977). The most prominent alteration effects are observed in these microlites. Reddish, hydrothermal (primary) alteration commonly occurs along grain margins and may or may not show fracture control. Brownish (secondary) alteration is confined to <20-μm-wide regions along fractures and is believed to be the result of weathering (Lumpkin and Ewing, 1985; Ewing, 1975; Van Wambeke, 1970).

Replacement units also contain microlite as an accessory phase. The microlites are enclosed in bladed albite and associated with minor lepidolite, muscovite, and quartz within the cleavelandite unit (Fig. 1d). Large euhedral crystals (up to 15 mm) occur where the unit replaces the beryl zone. They are often zoned from yellow cores to dark brown rims. Other crystals display an unusual mottled yellow/brown exterior coloration. In the core of the pegmatite, the cleavelandite unit mainly replaces the quartz–lath spodumene zone. Microlite is found in this unit as euhedral to subhedral crystals (up to 3 mm) ranging in color from pale yellow to black. Many crystals show this color change in core-to-rim zoning. Submillimeter yellow and brown microlites are associated with cleavelandite pseudomorphs after spodumene (Fig. 2). Crystals tend to be aligned near the edges of pseudomorphs where adjacent quartz is darker in color. Color zoning is not prevalent, but a few grains show nonconcentric zoning involving a light-to-dark color change toward the cleavelandite–quartz interface (Fig. 1c).

Microlite also occurs within a lepidolite-cleavelandite subunit in eastern extensions of the pegmatite dike (Chakoumakos, 1978). The microlite is distributed as brown to black, 0.5 to 5.0 mm, euhedral to subhedral crystals in a matrix of lepidolite, bladed albite, and quartz. Accessory columbite-tantalite completes the association.

Experimental procedures

X-ray diffraction studies

A variety of analyses was performed using either a Philips or a Scintag diffractometer and Cu$K\alpha$ radiation: (1) A suite of single crystals was hand picked from a microlite concentrate, mounted on a Gandolfi attachment, and X-rayed in a 114.6-mm Debye-Scherrer camera. Films were corrected for shrinkage, and lattice constants were refined by least-squares analysis. The crystals were then mounted and polished for electron-microprobe analysis. (2) Powder-diffractometer traces were recorded for larger specimens with the Philips unit. Patterns were calibrated with BaF_2(a = 0.6198 nm) as an external standard, and lattice constants were refined by least-squares analysis. (3) Powder-diffraction patterns for five microlites ranging from crystalline to metamict were collected with a Scintag diffractometer (see Fig. 12), and lattice constants were refined using the program LATCON (Scintag software). In addition, samples annealed during the course of TGA measurements were X-rayed and found to have recrystallized to microlite plus minor $CaTa_2O_6$ and $CaTa_4O_{11}$.

Transmission electron microscopy

Three microlite samples (highly crystalline, partially metamict, and fully metamict) were dispersed onto holey carbon grids in methanol. The samples were examined with a JEOL 2000 FX TEM operated at an accelerating potential of 200 keV. Standard bright-field (BF), selected-area diffraction (SAD), and high-resolution (HRTEM) techniques were employed. SAD patterns were calibrated using a gold film under the same instrumental conditions. A double-tilting stage was used to bring the [111] zone axis into the diffracting condition such that HRTEM images show primarily 0.6-nm (111) and 0.3-nm (222) fringes. Image resolution and magnification were checked using a graphitized carbon (0.34 nm) standard. HRTEM images were taken at magnifications of 410 000 or 500 000. The samples appeared to be stable for at least 10 min under normal operating conditions.

Thermogravimetric analysis

Water contents were estimated for a few samples using a DuPont 951 TGA and 990 Recorder. Samples weighing 10 to 20 mg were heated in air to 1000°C at a rate of 10°/min. The system was calibrated with a calcium oxalate standard using the same operating parameters. The calibration was checked by reweighing each sample after cooling to room temperature. The percentage of weight loss calculated in this way was usually within 5% of that measured.

Electron microprobe analysis

Over 200 microlite analyses have been obtained using an automated JEOL 733 operated at an accelerating voltage of 15 keV and a sample current of 20 nA. Standards include natural samples of microlite (F, Na, Ca, Nb, Ta), manganotantalite (Mn), stibiotantalite (Sb, Bi), benitoite (Ti, Ba), olivine (Fe), cerussite (Pb), pollucite (Cs), and cassiterite (Sn). Synthetic crystals of $CaWO_4$, YPO_4, $CePO_4$, $ThSiO_4$, and UO_2 were used for W, Y, Ce, Th, and U. Each element was counted until a relative standard deviation of 1.0% was reached, up to a maximum counting time of 30 s. To minimize volatilization induced by electron-beam heating, all analyses were performed with a beam diameter of 10 μm. Data were corrected for drift, deadtime, absorption, fluorescence, and atomic number effects using a theoretical (ZAF) procedure based on the program MAGIC IV (Colby, 1968). The complete set of analyses is presented in Table 1.[1] Average analyses (including H_2O) are given in Table 2, and representative analyses are grouped according to lithologic unit in Table 3.

Structural formulas

All microlite analyses were converted to a structural formula based on a total of 2.0 B-site cations (cf., Borodin and Nazarenko, 1957; Van Wambeke, 1970). This allows an estimate of the A-site vacancies for each analysis. The major problem in assigning a structural formula is determination of the oxidation state of Fe, which can enter either the A site (Fe^{2+}) or the B site (Fe^{3+}). Chemical analyses by C. O. Ingamells (in Jahns and Ewing, 1976) reported Fe as FeO and/or Fe_2O_3 in no systematic fashion; however, for all five analyses, FeO averages 0.07 and Fe_2O_3 averages 0.02 wt%. Consequently, we report all Fe as FeO and allocate it to the A site, which minimizes A-site vacancies. This effect will be slight since the Fe content is very low in most of the probe analyses. On the basis of chemical analyses in Jahns and Ewing (1976), all U is calculated as UO_3, which increases the calculated O content in the anion group and minimizes Y-site vacancies.

The amount of O, OH, and F can be calculated in conjunction with H_2O contents estimated by TGA. A major difficulty is the determination of whether the water is present as OH or molecular H_2O. Our TGA data alone are not sufficient in this respect. Water released at ca. 150°C is most likely molecular H_2O, but much of the water was released gradually up to 1000°C and cannot be distinguished as OH^- or molecular H_2O. Borodin and Nazarenko (1957) assumed a total of seven anions and calculated the amount of OH necessary to achieve charge balance. Excess water was allocated as H_2O. In general, this procedure is not strictly valid because of anion vacancies at the Y site [Pyatenko, 1959 (1960); Aleshin and Roy, 1962; Subramanian et al., 1983; Chakoumakos, 1984]. We calculate two end-member formulas that bracket the range of possible anion chemistries: one that maximizes OH and another that includes all water as molecular H_2O and maximizes Y-site vacancies (Table 2). For the analyses in which H_2O has not been estimated by TGA, a single formula is calculated and Y-site vacancies are allocated when F and O are less than 7.0 (Tables 1 and 3). Assumptions involved in calculating structural formulas mainly affect O, OH, and H_2O and Y-site vacancies. The reader should be aware of these uncertainties in the following discussion.

MICROLITE CHEMISTRY

General relationships

Excluding alteration effects, the major-element contents are not unusual when compared to analyzed microlites from other localities (Bonshtedt-Kupletskaya, 1966; Von Knorring and Fadipe, 1981; Lumpkin and Ewing, 1985; Von Knorring and Condliffe, 1984; Lumpkin, unpublished microprobe analyses). The typical ranges in values (in weight percent) are 60–78 Ta_2O_5, 2.5–12 Nb_2O_5, 0.0–3.2 TiO_2, 0–11 UO_3, 8–13 CaO, 2.0–5.5 Na_2O, 1.5–3.5 F, and 0.1–4.0 H_2O. The H_2O contents estimated by TGA are consistent with analytical totals of >95 wt% for analyses where H_2O is not determined (Tables 1 and 3). Major elements nearly cover the range of known microlite compositions.

Certain minor elements appear to be enriched or depleted relative to microlites from other localities. For example, SnO_2 is consistently below 0.05 wt%, reflecting the Sn-poor composition of the pegmatite melt-fluid. Other microlites typically contain SnO_2 in the 0.05–5.0 wt% range. The MnO content ranges up to 2.0 wt%, reflecting a Mn-rich melt-fluid which also crystallized spessartine and manganocolumbite. Other minor elements are probably near the average abundance level. BaO, Cs_2O, Y_2O_3, Bi_2O_3, and ThO_2 are typically below 0.10 wt%. Ce_2O_3, Sb_2O_3, and WO_3 are usually within the 0.1–0.4 wt% range. FeO and PbO have maximum concentrations of 1.5 and 4.5 wt%, respectively. In addition, ZrO_2 was analyzed in a few samples but was not present above the 0.03 wt% level. This may reflect a relatively high SiO_2 activity, which favored crystallization of zircon. In carbonatites, where the SiO_2 activity is relatively low, Zr oxides such as baddeleyite and zirconolite form instead, and the pyrochlore phase may contain up to ca. 10 wt% ZrO_2. Our data for WO_3 do not agree with partial microprobe analyses made by Suchomel (1976), who reported as much as 4.2 wt% WO_3.

Stoichiometry

B-site cations. Pentavalent Ta and Nb are the dominant cations occupying the octahedral B site (Fig. 3). The amount of Ta ranges from 1.35 to 1.85 and Nb ranges from 0.10 to 0.45 atoms per formula unit. Substitution of Ti is limited to a maximum of 0.25 atoms per formula unit. The contents of W and Sn rarely attain 0.01 and 0.003 atoms per formula unit, respectively.

[1] To receive a copy of Table 1, order Document AM-86-297 from the Business Office, Mineralogical Society of America, 1625 I Street, N.W., Suite 414, Washington, D.C. 20006. Please remit $5.00 in advance for the microfiche.

Table 2. Average electron-microprobe analyses for Harding pegmatite microlites with H_2O contents estimated by TGA (formulas based on $\Sigma B = 2.00$ include two possible anion distributions; see text)

	147		148		149		150		153		154		288	
WO_3	0.26		0.08		0.03		0.23		0.06		0.07		0.20	
Ta_2O_5	75.1		74.7		75.6		74.1		70.2		61.7		71.2	
Nb_2O_5	5.68		4.36		5.22		5.66		4.77		7.61		5.28	
TiO_2	0.02		0.03		0.20		0.05		0.40		0.90		0.62	
SnO_2	0.01		0.00		0.00		0.01		0.00		0.00		0.00	
ThO_2	0.03		0.04		0.00		0.04		0.00		0.10		0.05	
UO_3	0.00		2.20		0.69		1.84		9.07		10.0		3.07	
Y_2O_3	0.00		0.07		0.10		0.02		0.00		0.08		0.07	
Ce_2O_3	0.14		0.09		0.12		0.18		0.13		0.20		0.17	
Sb_2O_3	0.09		0.11		0.09		0.08		0.05		0.08		0.14	
Bi_2O_3	0.04		0.00		0.05		0.10		0.17		0.02		0.00	
MnO	0.03		0.19		0.06		0.03		0.09		0.54		0.16	
FeO	0.03		0.00		0.00		0.04		0.06		0.04		0.12	
CaO	10.4		11.0		11.6		9.65		8.62		10.5		11.9	
BaO	0.00		0.00		0.03		0.00		0.00				0.00	
PbO	0.04		0.03		0.02		0.10		1.85		0.29		0.06	
Na_2O	5.10		4.25		3.70		4.77		3.32		3.17		3.09	
Cs_2O	0.00		0.04		0.00		0.00		0.02		0.00		0.00	
F	3.41		2.04		2.44		2.51		1.25		1.43		1.65	
H_2O	0.1		1.1		0.7		1.2		1.2		4.0		3.2	
SUM	100.48		100.34		100.65		100.61		101.26		100.73		100.98	
O≡F	-1.43		-0.86		-1.02		-1.05		-0.52		-0.60		-0.69	
TOTAL	99.05		99.48		99.63		99.56		100.74		100.13		100.29	
W	0.006		0.002		0.001		0.005		0.001		0.002		0.005	
Ta	1.770		1.820		1.782		1.767		1.771		1.607		1.739	
Nb	0.223		0.177		0.204		0.225		0.200		0.328		0.214	
Ti	0.001		0.002		0.013		0.003		0.028		0.063		0.042	
Sn	0.000		0.000		0.000		0.000		0.000		0.000		0.000	
Th	0.001		0.001		0.000		0.001		0.000		0.002		0.001	
U	0.000		0.041		0.013		0.036		0.177		0.213		0.058	
Y	0.000		0.003		0.005		0.001		0.000		0.004		0.003	
Ce	0.004		0.003		0.004		0.006		0.004		0.007		0.006	
Sb	0.003		0.004		0.003		0.003		0.002		0.003		0.005	
Bi	0.001		0.000		0.001		0.002		0.004		0.000		0.000	
Mn	0.002		0.014		0.004		0.002		0.007		0.044		0.012	
Fe	0.002		0.000		0.000		0.002		0.005		0.003		0.009	
Ca	0.965		1.055		1.077		0.910		0.856		1.077		1.145	
Ba	0.000		0.000		0.000		0.000		0.000				0.000	
Pb	0.001		0.001		0.000		0.003		0.046		0.008		0.001	
Na	0.857		0.738		0.622		0.812		0.597		0.586		0.538	
Cs	0.001		0.002		0.000		0.000		0.001		0.000		0.000	
□A	0.16	0.16	0.14	0.14	0.27	0.27	0.22	0.22	0.30	0.30	0.05	0.05	0.22	0.22
O	5.92	5.95	6.00	6.00	5.94	6.00	5.95	6.00	6.00	6.00	6.56	6.28	6.00	6.00
O	0.00	0.00	0.08	0.29	0.00	0.11	0.00	0.11	0.25	0.56	0.00	0.57	0.00	0.38
OH	0.07	0.00	0.34	0.00	0.33	0.00	0.31	0.00	0.39	0.00	0.57	0.00	0.53	0.00
F	0.93	0.93	0.58	0.58	0.67	0.67	0.69	0.69	0.37	0.37	0.43	0.43	0.47	0.47
□Y	0.00	0.07	0.00	0.13	0.00	0.22	0.00	0.20	0.00	0.07	0.00	0.00	0.00	0.15
H_2O	0.00	0.03	0.12	0.33	0.04	0.20	0.20	0.35	0.06	0.37	0.99	1.28	0.69	0.96

A-site cations. The major cations in the eight-coordinated A site are Ca and Na (Fig. 4). Typical ranges for these cations are 0.85 to 1.30 for Ca and 0.30 to 0.95 for Na. No other cations achieve 20% of the A-site total; therefore, all of the Harding samples are microlite, as defined by Hogarth (1977). The minor elements U, Mn, Fe, and Pb approach maximum amounts of 0.25, 0.15, 0.06, and 0.10 atoms per formula unit, respectively. Fe is below 0.01 in most of the formulas. The maximum content of Sb is 0.02 atoms per formula unit. Y, Ce, Bi, and Cs are usually less than 0.01 and Ba is below 0.003 atoms per formula unit. Based on total A-site cations, the number of vacancies ranges from 0.0 to nearly 0.4. A few of the analyses of hydrothermally altered microlites from the microcline-spodumene zone give A-site totals in excess of 2.00 (up to 2.13). These A-site excesses could be due to either B-site vacancies or an A-site cation located at the B site. Because Fe and Sb are low in these samples, the most likely candidates are Mn^{3+} and U^{6+} (Subramanian et al., 1983; Chakoumakos, 1984; Chakoumakos and Ewing, 1985). Although site occupancy determinations are needed to prove this, enough Mn is present to account

Table 3. Representative electron-microprobe analyses of microlites from lithologic units of the Harding pegmatite (formulas based on $\Sigma B = 2.00$)*

	Quartz - Lath Spodumene Zone						Cleavelandite Unit (repl. Quartz-Lath Spodumene Zone)					
	261c	261r	271c	271r	272c	272r	267	265	P03.1c	P03.1r	P04c	P04r
WO_3	0.14	0.16	0.38	0.28	0.14	0.14	0.25	0.23	0.48	0.25	0.38	0.29
Ta_2O_5	75.1	67.7	74.4	77.3	74.7	74.9	75.2	67.4	72.8	62.0	76.0	73.4
Nb_2O_5	6.08	9.35	5.66	2.72	5.27	5.01	5.51	9.96	7.49	10.5	5.64	4.48
TiO_2	0.03	0.30	0.07	0.42	0.00	0.16	0.02	0.47	0.03	1.59	0.03	0.67
SnO_2	0.00	0.00	0.01	0.04	0.00	0.00	0.03	0.00	0.01	0.02	0.00	0.03
ThO_2	0.00	0.00	0.03	0.00	0.07	0.00	0.05	0.04	0.00	0.04	0.03	0.01
UO_3	0.06	2.18	0.31	0.66	0.03	0.78	0.00	2.75	1.28	4.23	0.05	2.61
Y_2O_3	0.00	0.00	0.06	0.05	0.05	0.08	0.02	0.03	0.09	0.07	0.06	0.07
Ce_2O_3	0.25	0.21	0.00	0.05	0.12	0.08	0.12	0.16	0.21	0.11	0.14	0.21
Sb_2O_3	0.17	0.31	0.11	0.19	0.09	0.14	0.12	0.15	0.27	0.48	0.14	0.23
Bi_2O_3	0.12	0.20	0.12	0.00	0.09	0.16	0.02	0.06	0.12	0.00	0.07	0.06
MnO	0.03	0.10	0.03	0.12	0.20	0.06	0.02	0.18	0.00	0.36	0.00	0.02
FeO	0.00	0.04	0.00	0.01	0.00	0.00	0.00	0.00	0.14	0.34	0.05	0.11
CaO	10.7	11.0	11.7	12.8	11.8	11.7	11.1	11.4	10.4	13.1	10.4	10.5
BaO	—	—	0.00	0.00	—	—	—	0.01	0.00	0.01	0.00	0.01
PbO	0.00	0.03	0.03	0.03	0.00	0.01	0.03	0.12	0.06	0.10	0.03	0.07
Na_2O	5.28	4.68	4.38	2.25	4.34	4.27	5.57	4.26	5.09	2.90	5.24	4.68
Cs_2O	0.04	0.00	0.00	0.02	0.00	0.00	0.00	0.00	0.01	0.00	0.03	0.02
F	3.23	2.33	2.94	2.45	3.03	2.47	3.40	2.25	2.88	2.12	3.35	2.41
SUM	101.23	98.59	100.23	99.39	99.84	99.96	101.46	99.47	101.36	98.22	101.64	99.88
O≡F	-1.36	-0.98	-1.23	-1.03	-1.27	-1.04	-1.43	-0.95	-1.21	-0.89	-1.41	-1.01
TOTAL	99.87	97.61	99.00	98.36	98.57	98.92	100.03	98.52	100.15	97.33	100.23	98.87
W	0.003	0.004	0.008	0.006	0.003	0.003	0.006	0.005	0.011	0.006	0.008	0.007
Ta	1.758	1.608	1.764	1.856	1.787	1.788	1.776	1.577	1.697	1.474	1.771	1.768
Nb	0.237	0.369	0.223	0.109	0.210	0.199	0.216	0.387	0.290	0.415	0.218	0.179
Ti	0.002	0.020	0.005	0.028	0.000	0.011	0.001	0.030	0.002	0.105	0.002	0.045
Sn	0.000	0.000	0.000	0.001	0.000	0.000	0.001	0.000	0.000	0.001	0.000	0.001
Th	0.000	0.000	0.001	0.000	0.001	0.000	0.001	0.001	0.000	0.001	0.001	0.000
U	0.001	0.040	0.006	0.012	0.001	0.014	0.000	0.050	0.023	0.078	0.001	0.048
Y	0.000	0.000	0.003	0.002	0.002	0.004	0.001	0.001	0.004	0.003	0.003	0.003
Ce	0.008	0.007	0.000	0.002	0.004	0.003	0.004	0.005	0.007	0.004	0.004	0.007
Sb	0.006	0.011	0.004	0.007	0.003	0.005	0.004	0.005	0.010	0.017	0.005	0.008
Bi	0.003	0.005	0.003	0.000	0.002	0.004	0.000	0.001	0.003	0.000	0.002	0.001
Mn	0.002	0.007	0.002	0.009	0.015	0.004	0.001	0.013	0.000	0.027	0.000	0.002
Fe	0.000	0.003	0.000	0.001	0.000	0.000	0.000	0.000	0.010	0.025	0.004	0.008
Ca	0.987	1.029	1.093	1.210	1.112	1.100	1.032	1.051	0.955	1.227	0.955	0.996
Ba	—	—	—	0.000	0.000	—	—	0.000	0.000	0.000	0.000	0.000
Pb	0.000	0.001	0.001	0.001	0.000	0.000	0.001	0.003	0.001	0.002	0.001	0.002
Na	0.881	0.792	0.740	0.385	0.740	0.726	0.938	0.711	0.846	0.491	0.870	0.804
Cs	0.001	0.000	0.000	0.001	0.000	0.000	0.000	0.000	0.000	0.000	0.001	0.001
□A	0.11	0.11	0.15	0.37	0.12	0.14	0.02	0.16	0.14	0.12	0.15	0.12
O	6.02	6.26	6.09	6.11	6.10	6.19	6.05	6.27	6.11	6.41	5.97	6.22
F	0.88	0.64	0.81	0.68	0.84	0.69	0.93	0.61	0.78	0.59	0.91	0.68
□Y	0.10	0.10	0.10	0.21	0.06	0.12	0.02	0.12	0.11	0.00	0.09	0.10
dose	0.026	0.90	0.12	0.27	0.013	0.032	<0.01	1.1	0.51	1.7	0.02	1.1
dpa	0.3	11	1	3	0.2	4	<0.1	14	6	21	0.3	13

* c = core, r = rim, p = primary alteration, s = secondary alteration, dose x 10^{17} alphas/mg, dpa = displacements per atom.

for ΣA in excess of 2.00 in each case and is positively correlated with ΣA. Furthermore, the ionic radius (Shannon, 1976) of Mn^{3+}(r_B = 0.0645 nm) is nearly identical to those of Nb^{5+} and Ta^{5+}(r_B = 0.064 nm). The radius of U^{6+} is significantly larger (r_B = 0.073 nm).

Anion group. The only anion determined by analysis was F, which ranges from 0.1 to 0.9 atoms per formula unit. The calculated amount of O ranges from 5.9 to 6.9 atoms per formula unit. Formulas presented in Table 2 bracket the OH content at 0.0–0.6 atoms and H_2O at 0.0–1.3 molecules per formula unit. The maximum number of Y-site vacancies approaches 0.4. ΣY tends to be greater than 1.00 where ΣA exceeds or is near 2.00. The highest contents of F occur in microlites from the quartz–lath spodumene zone and the cleavelandite unit which approach stoichiometric $NaCa(Ta_{1.8}Nb_{0.2})O_6F$. Microlites from lepidolite pods near the base of the quartz–lath spodumene zone are virtually identical in composition. The most unusual microlites are rich in Pb and poor in F. They occur in the microcline-spodumene zone, approaching the composition $\square^{A}_{0.4}Na_{0.4}Ca_{0.9}Pb_{0.1}Mn_{0.1}U^{6+}_{0.1}(Ta_{1.7}Nb_{0.3})O_{6.6}F_{0.1}\square^{Y}_{0.3}\cdot 1.2H_2O$ (H_2O estimated by difference).

Alteration effects

Processes of geochemical alteration are generally divided into primary (hydrothermal) and secondary (weathering) types (e.g., Van Wambeke, 1970; Ewing, 1975). For the complex, AB_2O_6, Ti-Nb-Ta oxides Ewing (1975) ob-

Table 3—*Continued*

	Lepidolite - Cleavelandite Subunit					Cleavelandite Unit (repl. Beryl Zone)					Microcline - Spodumene Unit					
	P02.1c	P02.1r	P02.2	P02.2s	P07.1	P01.1	P05.1c	P05.1r	P21.1	P.21.1	269	269	P17.1	P17.1p	264	264p
WO_3	0.25	0.00	0.12	0.06	0.13	0.08	0.35	0.31	0.00	0.10	0.53	0.48	0.27	0.04	0.32	0.00
Ta_2O_5	66.9	59.4	68.4	68.4	66.1	72.1	74.6	59.1	70.3	75.2	64.1	65.2	66.5	61.1	73.5	72.3
Nb_2O_5	7.45	10.1	7.52	6.03	7.54	4.74	5.71	10.2	8.38	3.44	7.67	7.34	7.85	9.15	5.63	5.43
TiO_2	0.05	1.00	0.72	0.65	0.94	1.20	0.11	3.23	0.02	0.37	0.09	0.07	0.12	0.26	0.14	0.51
SnO_2	0.01	0.01	0.00	0.01	0.02	0.06	0.06	0.02	0.00	0.00	—	—	0.00	0.00	—	—
ThO_2	0.06	0.07	0.04	0.00	0.05	0.17	0.00	0.06	0.00	0.01	—	—	0.00	0.00	—	—
UO_3	7.44	9.40	4.26	3.93	6.51	3.46	0.55	7.26	2.17	2.27	7.50	7.96	8.22	7.65	2.15	2.45
Y_2O_3	0.03	0.03	0.08	0.10	0.11	0.09	0.10	0.08	0.07	0.03	—	—	0.04	0.04	—	—
Ce_2O_3	0.11	0.15	0.16	0.22	0.19	0.13	0.26	0.23	0.06	0.13	—	—	0.19	0.15	—	—
Sb_2O_3	0.10	0.25	0.18	0.20	0.10	0.13	0.17	0.38	0.05	0.12	0.17	0.17	0.07	0.07	0.13	0.27
Bi_2O_3	0.00	0.01	0.07	0.06	0.00	0.00	0.00	0.00	0.00	0.03	—	—	0.00	0.00	—	—
MnO	0.24	0.34	0.13	0.15	0.41	0.27	0.00	0.70	0.08	0.33	1.13	0.75	0.19	1.05	0.22	0.88
FeO	0.29	0.70	0.17	0.33	0.46	0.44	0.09	0.43	0.01	0.30	0.05	0.03	0.02	0.03	0.00	0.42
CaO	9.57	9.83	10.7	6.10	11.6	11.3	11.4	11.4	11.2	10.9	8.52	11.9	9.23	11.6	11.2	13.9
BaO	0.00	0.03	0.00	0.05	0.03	0.04	0.03	0.00	0.00	0.02	—	—	0.00	0.00	—	—
PbO	0.19	0.26	0.11	0.17	0.22	0.09	0.18	1.19	0.06	0.06	4.27	1.62	0.25	0.19	0.33	0.23
Na_2O	3.42	3.23	3.94	0.55	2.68	3.57	4.58	2.76	4.28	3.53	2.16	1.88	3.95	3.01	4.59	2.41
Cs_2O	0.00	0.00	0.01	0.00	0.00	0.12	0.01	0.00	0.02	0.01	—	—	0.02	0.00	0.00	0.00
F^2	1.62	1.46	2.00	0.67	1.42	2.15	3.17	1.35	2.63	2.32	0.20	0.53	1.47	1.61	2.36	1.53
SUM	97.73	96.27	98.61	87.68	98.51	100.14	101.37	98.70	99.33	99.17	96.39	97.93	98.39	95.95	100.57	100.33
O≡F	-0.68	-0.61	-0.84	-0.28	0.60	-0.90	-1.33	-0.57	-1.10	-0.97	-0.08	-0.22	-0.62	-0.68	-0.99	-0.64
TOTAL	97.05	95.65	97.77	87.40	97.91	99.24	100.04	98.13	98.23	98.20	96.31	97.91	97.77	95.27	99.58	99.69
W	0.006	0.000	0.003	0.001	0.003	0.002	0.008	0.007	0.000	0.000	0.013	0.012	0.006	0.001	0.007	0.000
Ta	1.679	1.504	1.649	1.704	1.624	1.728	1.759	1.386	1.668	1.833	1.652	1.671	1.660	1.586	1.759	1.748
Nb	0.311	0.425	0.301	0.250	0.308	0.189	0.224	0.397	0.331	0.139	0.329	0.313	0.326	0.395	0.224	0.218
Ti	0.004	0.071	0.047	0.045	0.064	0.080	0.007	0.209	0.001	0.025	0.006	0.005	0.008	0.019	0.009	0.034
Sn	0.000	0.000	0.000	0.000	0.001	0.002	0.002	0.001	0.000	0.000	—	—	0.000	0.000	—	—
Th	0.001	0.001	0.001	0.000	0.001	0.003	0.000	0.001	0.000	0.000	—	—	0.000	0.000	—	—
U	0.144	0.184	0.079	0.076	0.123	0.064	0.010	0.131	0.040	0.043	0.149	0.157	0.158	0.153	0.040	0.046
Y	0.001	0.001	0.004	0.005	0.005	0.004	0.005	0.004	0.003	0.001	—	—	0.002	0.002	—	—
Ce	0.004	0.005	0.005	0.007	0.006	0.004	0.008	0.007	0.002	0.004	—	—	0.006	0.005	—	—
Sb	0.004	0.010	0.007	0.008	0.004	0.005	0.006	0.014	0.002	0.004	0.007	0.007	0.003	0.003	0.005	0.010
Bi	0.000	0.000	0.001	0.001	0.000	0.000	0.000	0.000	0.000	0.001	—	—	0.000	0.000	—	—
Mn	0.019	0.027	0.010	0.012	0.031	0.020	0.000	0.051	0.006	0.025	0.091	0.060	0.015	0.085	0.016	0.066
Fe	0.022	0.055	0.013	0.025	0.035	0.032	0.007	0.031	0.001	0.022	0.004	0.002	0.002	0.002	0.000	0.031
Ca	0.946	0.981	1.014	0.599	1.123	1.067	1.059	1.053	1.047	1.047	0.865	1.201	0.907	1.186	1.056	1.324
Ba	0.000	0.001	0.000	0.002	0.001	0.001	0.001	0.000	0.000	0.001	—	—	0.000	0.000	—	—
Pb	0.005	0.007	0.002	0.004	0.005	0.002	0.004	0.028	0.001	0.001	0.109	0.041	0.006	0.005	0.008	0.006
Na	0.612	0.583	0.677	0.098	0.469	0.610	0.770	0.461	0.724	0.613	0.397	0.343	0.703	0.557	0.783	0.415
Cs	0.000	0.000	0.000	0.000	0.000	0.005	0.000	0.000	0.001	0.000	—	—	0.001	0.000	—	—
□A	0.24	0.15	0.19	1.16	0.20	0.18	0.13	0.22	0.17	0.24	0.38	0.19	0.20	0.00	0.09	0.10
O	6.51	6.57	6.34	5.83	6.59	6.31	6.08	6.54	6.18	6.21	6.70	6.88	6.56	6.78	6.27	6.55
F	0.47	0.43	0.56	0.19	0.41	0.60	0.87	0.37	0.73	0.66	0.06	0.16	0.43	0.49	0.66	0.43
□Y	0.02	0.00	0.10	0.81	0.00	0.09	0.05	0.09	0.09	0.13	0.24	0.00	0.01	0.00	0.07	0.02
dose	3.1	3.9	1.7	1.9	2.7	1.4	0.22	3.0	0.89	0.93	3.1	3.3	3.3	3.2	0.87	0.98
dpa	40	51	21	24	35	18	3	37	11	12	44	45	44	42	11	13

* c = core, r = rim, p = primary alteration, s = secondary alteration, dose x 10^{17} alphas/mg, dpa = displacements per atom.

served consistent increases in Ca associated with primary alteration. Samples thought to reflect secondary alteration showed significant leaching of A-site cations such as Y, REE, U, and Th and increased H_2O content. Van Wambeke (1970) found similar results for a uranpyrochlore and a betafite from Madagascar.

Lumpkin and Ewing (1985) used a combination of scanning electron microscopy, electron-microprobe analysis, and TGA to characterize altered pyrochlores, betafites, and microlites. Four Harding pegmatite microlites were included. In general, the results showed that primary alteration produced minor increases in Fe and Mn, decreases in Na, and variable to minor changes in Ca, F, H_2O, and A-site vacancies. Secondary alteration resulted in leaching of Na, Ca, and F, with extensive hydration (up to 12 wt% H_2O). This process maximizes the number of A and Y vacancies tolerated by the pyrochlore structure and leads to cation exchange for small amounts of large cations like K, Sr, Ba, Pb, Bi, and Cs (Harris, 1965; Van Wambeke, 1978; Saffiannikoff and Van Wambeke, 1961; Von Knorring and Fadipe, 1981; Lumpkin and Ewing, 1985).

Electron-microprobe analyses of altered and unaltered areas of Harding microlites are given in Table 3. Specimens showing primary alteration (153, 154, 260, 264, 269, P07.1, P15.1, P17.1, P18.1) give consistent increases in Mn, Ca, and O in the structural formula. Increasing Ca supports the findings of Van Wambeke (1970) and Ewing (1975). The typical increases in these elements are 0.05–0.10 Mn, 0.20–0.40 Ca, and 0.10–0.40 O atoms per formula unit. The content of Fe increases in some of the samples by as much as 0.03 atoms per formula unit. Similar increases in Ti and U compensated by decreasing Ta and Nb were noted in a few cases, but could be the result of alteration superimposed on original compositional heterogeneity. The F content remains approximately constant. Considering analytical totals, the probe data indicate that total H_2O also remains nearly constant, except in a few cases (P15.1, P07.1) where an increase of up to 2 wt% is inferred. This is equivalent to 0.7 OH anions or 0.35 H_2O molecules in the formula. The amount of Pb is constant if the unusual Pb-rich grains (269) are considered not to have resulted from alteration (see Fig. 1f). Primary alteration also leads to consistent decreases of 0.10–0.35 Na, 0.1–0.4 $\square^A$, and 0.2–0.4 $\square^Y$. As noted above, some of the analyses suggest that Mn might be located at the B site. If so, the inferred decreases in A and Y vacancies would be diminished by 0.1–0.2.

Microprobe analyses of secondary alteration (weathering) adjacent to fractures were obtained in a few of the samples (153, 269, P02.2). Pronounced decreases of up to 0.7 Na, 0.6 O, 0.5 Ca, and 0.5 F atoms per formula unit are observed. The amount of Pb decreases by as much as 0.03 atoms per formula unit. These changes are accompanied by increases in vacancies of up to 0.9 $\square^A$ and 0.7 $\square^Y$. Minor increases in Mn and Fe occur, but significant increases in Ba, Pb, Bi, and Cs were not observed. Low analytical totals of the probe results suggest total H_2O contents of 8–13 wt%, consistent with TGA results on other pyrochlores, betafites and microlites (Lumpkin and Ewing, 1985; Lumpkin, unpub. data). Assuming an H_2O content of 12 wt%, a typical formula is $\square^A_{1.2}\,Ca_{0.6}\,Na_{0.1}\,U_{0.1}$-$(Ta_{1.7}Nb_{0.25}Ti_{0.05})O_{5.8}F_{0.2}\square^Y_{1.0}\cdot 3.5H_2O$.

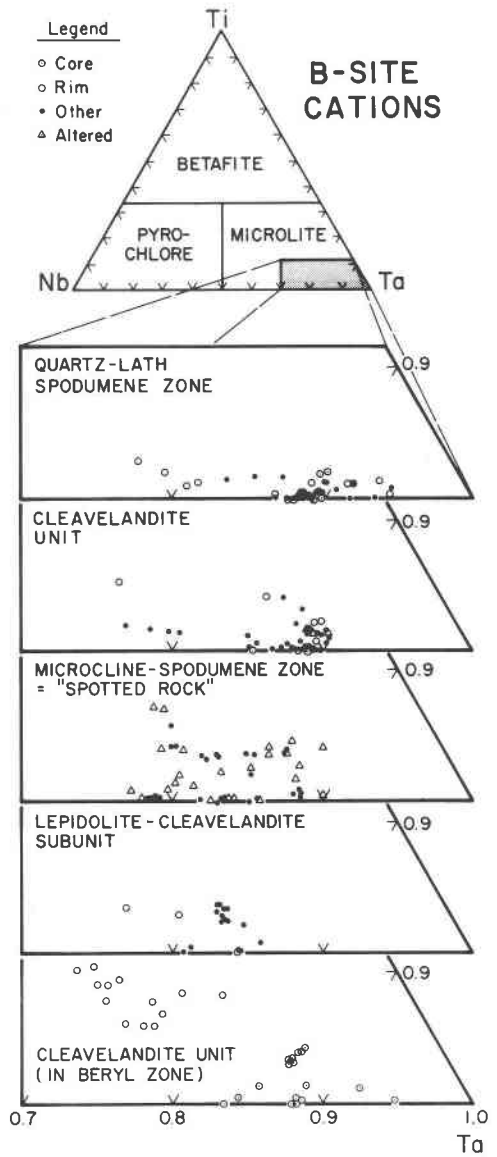

Fig. 3. Major-element B-site chemistry by lithologic unit for the Harding pegmatite microlites. Minor amounts of Sn and W are excluded. The points labeled *other* include unzoned grains and analytical points between the core and rim of zoned grains.

Intracrystalline zoning patterns

As expected from the occurrence of distinct color zoning, many of the Harding microlites show core-to-rim variation in both major and minor elements. Three general types of zoning patterns have been observed: (1) Crystals in which Nb, Na, and F decrease and Ta, Ca, U, Ti, and H_2O increase from core to rim. Increasing H_2O con-

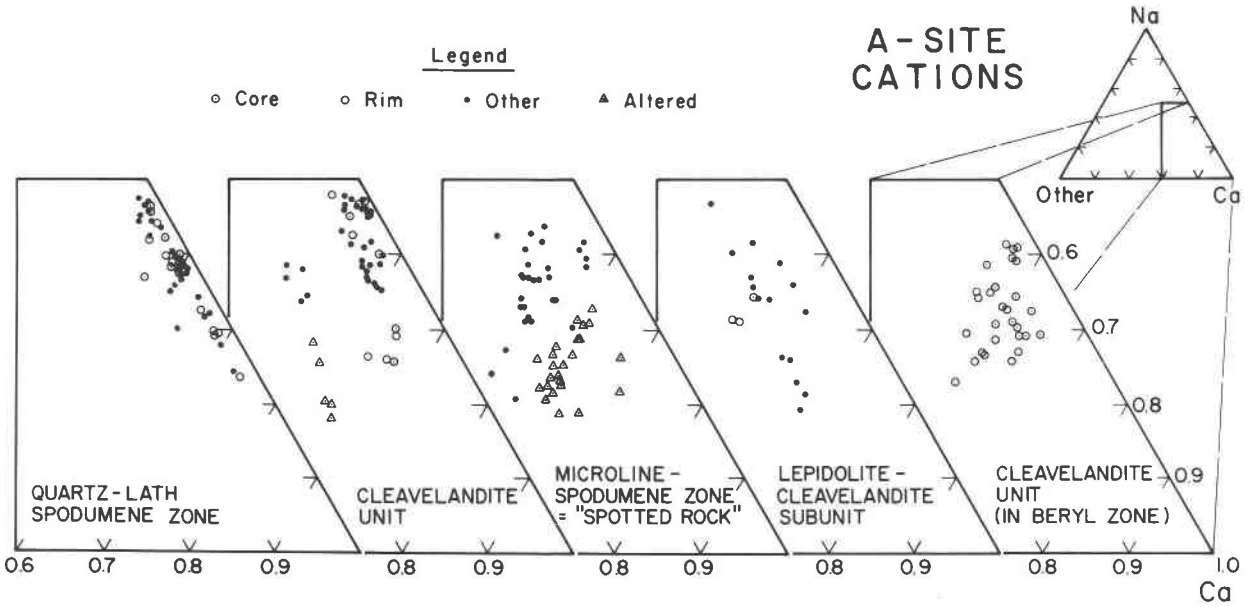

Fig. 4. A-site chemistry by lithologic unit for the Harding pegmatite microlites. The ternary end-member *other* includes Th, U^{6+}, Y, Ce, Sb, Bi, Mn, Fe^{2+}, Ba, Pb, and Cs. The points labeled *other* include unzoned grains and analytical points between the core and rim of zoned grains.

tent is inferred from lower analytical totals of rim compositions. (2) Microlites with cores relatively rich in Nb, Ta, Na, and F and rims relatively rich in U, Ti, and H_2O. Ca content remains fairly constant as does the Nb/Ta ratio. (3) Grains of microlite that have decreasing contents of Ta, Na, and F coupled with increasing amounts of Nb, Ca, U, Ti, and H_2O from core to rim.

In addition, the minor elements Mn, Fe, Sb, and Pb tend to be enriched in crystal rims. U-Ti and Na-F have a close positive correlation in all three types of zoning. In zoning patterns 1 and 3, Nb-Ta and Ca-Na show a negative correlation. Note also that these two patterns differ mainly in the reversed core-to-rim behavior of Nb and Ta. Zoning types 1 and 2 are characteristic of microlites from the quartz–lath spodumene zone. Zoning pattern 3 is typical of microlites from the cleavelandite unit, lepidolite–cleavelandite subunit and cleavelandite pseudomorphs after spodumene.

Zoning trends observed in this study reflect the general trends suggested by Von Knorring and Fadipe (1981). Except for Nb-Ta in zoning type 1 and Ca in types 1 and 3, the core-to-rim variations contrast with those of microlites from the pocket zone of the Himalaya (California) pegmatite system (Foord, 1976). In all cases, Foord (1976) found decreasing U, Ti, and possibly Sb and corresponding increases in Ta, Ca, Na, and F.

Substitution schemes

Correlations among the full set of chemical variables have been examined. These are used below in conjunction with zoning patterns and alteration effects to construct end members for characterizing the chemical changes. We do not mean to imply that such end members actually occur. In turn, end-member compositional variations allow a determination of substitution mechanisms. The simplest case, Ta-Nb substitution, is obvious from intracrystalline zoning and has a correlation coefficient (r) of −0.92. Other substitutions are more complex and require detailed evaluation in terms of end-member compositions.

A convenient starting point is the ideal microlite composition $NaCa(Ta,Nb)_2O_6F$ or $A^{1+}A^{2+}B_2^{5+}X_6^{2-}Y^-$. This component accounts for 40–95% of the composition of the samples and is supported by positive correlation of Na-F shown in Figure 5 (r = 0.71). Much of the scatter in this plot results from primary alteration, in which Na decreases as F remains nearly constant. Intracrystalline zoning patterns show a close positive correlation of Na-F. Variation of divalent cations Ca, Mn, and Pb can be accounted for by the end members $A_2^{2+}B_2^{5+}O_7$ and $A^{2+}B_2^{5+}O_6$ (cf., Borodin and Nazarenko, 1957). Together they account for 10–50% of the compositional variation. The second end member is supported by formation of minor amounts of $CaTa_2O_6$ during TGA analysis and the positive correlation of $\square^A$–$\square^Y$ shown in Figure 6 (r = 0.80). Some of the scatter above the 1:1 variation line may be due to overestimation of U as U^{6+}. Calculation of some of the U as U^{4+} would increase $\square^Y$ at constant $\square^A$. The $A_2^{2+}B_2^{5+}O_7$ component is strongly supported by elemental variations resulting from primary alteration. The possibility of having Mn^{3+} at the B site raises the potential for end-member components like Ca_2TaMnO_6, $CaU^{4+}TaMnO_7$, or even $U^{6+}TaMnO_7$.

The scatter plot of A-site vacancies versus Y-site vacancies (Fig. 6) is somewhat misleading in that no OH has been allocated to the Y site (because H_2O was not

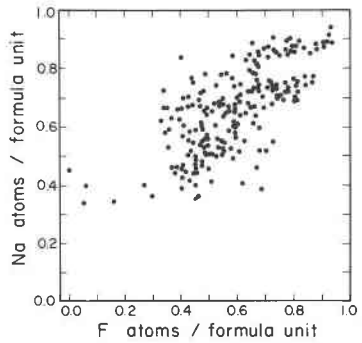

Fig. 5. Na versus F in atoms per formula unit for the Harding pegmatite microlites.

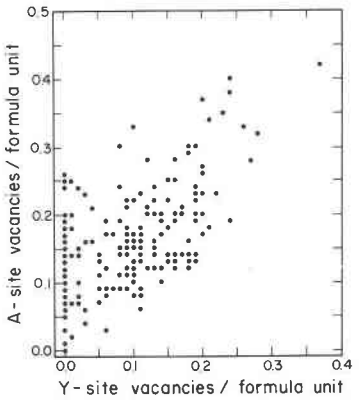

Fig. 6. A-site vacancies versus maximum Y-site vacancies per formula unit for the Harding pegmatite microlites.

determined for these analyses). For the mean analyses for which H_2O was determined (Table 2), there is enough water to completely fill the Y site with hydroxyl and in many cases to have excess molecular H_2O. Not determining H_2O/OH maximizes the Y-site vacancies, whereas allocating as much OH as possible to the Y site will minimize the Y-site vacancies. Therefore, to establish a correlation between A-site and Y-site vacancies, as proposed by Pyatenko (1959) and Aleshin and Roy (1962), hydroxyl and molecular H_2O must be determined, otherwise the correlation is dependent on assumptions in the calculation of the structural formula.

An inverse correlation between U and F was found (Fig. 7). The wet chemical analyses of microlites by C. O. Ingamells reported in Jahns and Ewing (1976) indicate that the Harding microlites have high U^{6+}/U^{4+} ratios. In the absence of wet chemical analyses for these samples, we assume that all the uranium is U^{6+}. The correlation, between U^{6+} and F is noteworthy because it supports the proposition that U^{6+} at the cubic A site in the pyrochlore structure is much like the uranyl group (UO_2^{2+}) and its characteristic coordination polyhedron, which has been suggested by Greegor et al. (1985b) based on extended X-ray absorption fine structure of UL-edges in metamict and annealed pyrochlore. The uranyl group is a common structural unit of many uranium compounds and is also stable in the aqueous environment. The uranyl ion is linear with U–O distances shorter than the sum of radii for O^{2-} and U^{6+}. Four, five, or six ligand atoms typically lie in the equatorial plane of the O–U–O group, with these U–O distances longer than radii sums. In comparison, the rhombohedrally distorted cubic A site of pyrochlore has a similar structure, with two short bonds in a linear Y–A–Y arrangement and a puckered equatorial girdle of six long A–X bonds (Chakoumakos, 1984, Subramanian et al., 1983); see inset of Figure 7. With Y–A–Y as the uranyl group, the amount of F at the Y site will be inversely correlated with U^{6+} (Fig. 7). The large amount of scatter in Figure 7 is expected because hydroxyls and vacancies also substitute for F at the Y site. The lines plotted in Figure 7 illustrate two theoretical relationships between U^{6+} and F at the Y site, assuming that each U^{6+} belongs to a uranyl group at the A site and the maximum F at the Y site is 0.7 atoms (the difference being vacancies or hydroxyl). The first line (shallower slope) is for two Y-site oxygens for each U^{6+}, which would be expected for low concentrations of U (i.e., widely scattered UO_8 polyhedra). The second line (steeper slope) is one Y-site O for each U^{6+}, which would be the limit approached as the U content increased and UO_8 polyhedra shared corners (Y-site oxygens). Actually, an infinite number of lines can be drawn parallel to those in Figure 7, each for a different amount of vacancy plus OH substitution at the Y site. Note that the data roughly trend along the relationship of U^{6+} = 2(Y-site oxygens), as expected for low U content. The correlation should shift toward the relationship of U^{6+} = (Y-site oxygens) as the U content increases, finally

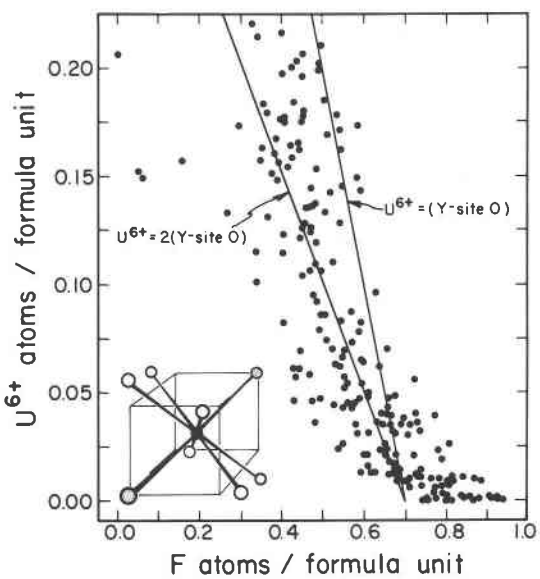

Fig. 7. U versus F in atoms per formula unit for the Harding microlites. The two lines are theoretical relationships assuming all the U is hexavalent and requires oxygen in the Y site; see text for discussion. The insert illustrates the A-site coordination relative to a reference cube in the pyrochlore structure.

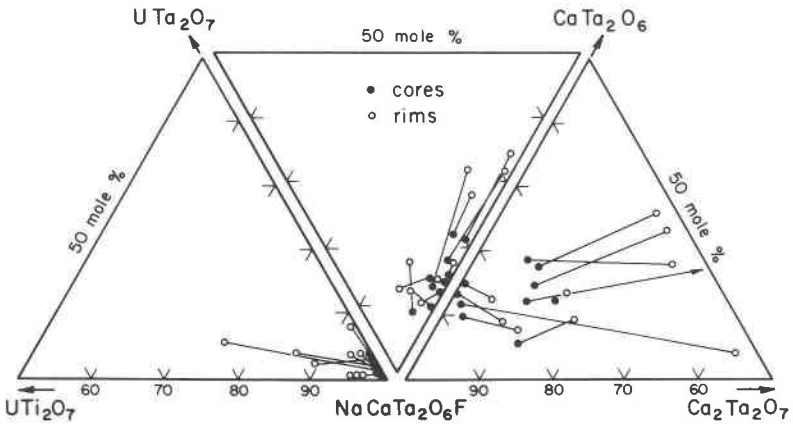

Fig. 8. Intracrystalline chemical variations (zoning) plotted in terms of hypothetical end-member compositions. Mn and Pb are included with Ca, and Nb with Ta.

reaching the approximate limits of 0.4 and 0.6 atoms per formula unit for a defect ($A\square B_2O_7$) and ideal ($A_2B_2O_7$) microlite, respectively. Note that the U^{6+} values may be slightly overestimated in calculating all the U (4+ and 6+) as hexavalent. With increased hexavalent U at the A site, increased divalent anions are needed in the Y site to preserve electrostatic neutrality as well as possible; alternatively, the stable uranyl group simply persists as a fundamental unit in the crystal. An alternative diagram that illustrates this same relationship is a plot of U^{6+} versus the O content of the Y site ($r = 0.93$). However, the true values of the Y-site O are dependent on the water or hydroxyl content and the specific method of calculating the structural formula.

Other microlite end members involve the incorporation of U at the A site and Ti at the B site. A close positive correlation of U-Ti in zoning patterns can be used to postulate the components $CaUTi_2O_7$, $U^{4+}TaTiO_6F$, and $U^{6+}Ti_2O_7$ (or $U^{4+}Ti_2O_6$). The first two are excluded owing to a lack of correlation observed for Ca-U and the negative correlation found for U-F ($r = -0.79$). The U-F data plotted in Figure 7 are consistent with the structure of the uranyl group if U is considered to have entered the structure as U^{6+} at the A site. However, data for A and Y vacancies (Fig. 6) suggest that at least some of the U was originally incorporated as U^{4+}. Furthermore, when we form the component $U^{6+}Ti_2O_7$ (or $U^{4+}Ti_2O_6$), there is usually excess U remaining that must be considered to be U^{4+} in a component like $U^{4+}Ta_2O_7$ (disregarding primary alteration effects). Lacking more precise data on the initial oxidation state of U, we arbitrarily use the end members $U^{6+}Ti_2O_7$ and $U^{4+}Ta_2O_7$ for purposes of plotting in Figures 8 and 9. These account for up to 30% of the observed chemical variation. Intracrystalline zoning patterns are displayed in Figure 8 based on the end members $NaCaTa_2O_6F$, $Ca_2Ta_2O_7$, $CaTa_2O_6$, UTa_2O_7, and UTi_2O_7. In all cases, Mn and Pb are included with Ca and Nb with Ta. Core-to-rim trends indicate increases in the components $Ca_2Ta_2O_7$, $CaTa_2O_6$, UTa_2O_7, and UTi_2O_7 relative to $NaCaTa_2O_6F$. The substitution schemes derived from these trends are listed in Table 4 in order of decreasing importance. Alteration effects have been evaluated on the same basis. Figure 9 shows that the end members UTa_2O_7 and $Ca_2Ta_2O_7$ increase in relation to $NaCaTa_2O_6F$. In

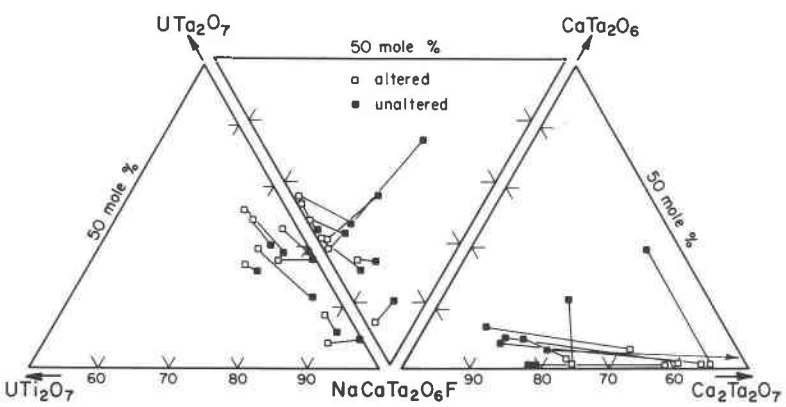

Fig. 9. Primary (hydrothermal) alteration effects plotted in terms of hypothetical end-member compositions. Mn and Pb are included with Ca, and Nb with Ta. Apparent increases in U end members are the result of major increases in the $Ca_2Ta_2O_7$ component.

Table 4. Substitution schemes for microlites from the Harding pegmatite

Zoning Trends	Primary Alteration
$^{B}Nb \rightarrow {}^{B}Ta$	$^{A}Ca^{Y}O \rightarrow {}^{A}Na^{Y}F$
$^{B}Ta \rightarrow {}^{B}Nb$	$^{A}Ca^{Y}O \rightarrow {}^{A}\square^{Y}\square$
$^{A}Ca^{Y}O \rightarrow {}^{A}Na^{Y}F$	if Mn^{3+}:
$^{A}\square^{Y}\square \rightarrow {}^{A}Na^{Y}F$	$^{A}U^{6+}\ {}^{B}Mn \rightarrow {}^{A}U^{4+}\ {}^{B}Ta$
$^{A}\square^{A}U^{B}Ti_2{}^{Y}O \rightarrow {}^{A}Na^{A}Ca^{B}Ta_2{}^{Y}F$	
$^{A}\square^{A}U^{Y}O \rightarrow {}^{A}Na^{A}Ca^{Y}F$	

some cases, UTi_2O_7 increases relative to $NaCaTa_2O_6F$, and $Ca_2Ta_2O_7$ increases with respect to $CaTa_2O_6$. Because of the major substitution of $Ca_2Ta_2O_7$, increases in the U components are more apparent than real. Corresponding substitution schemes are ranked in Table 4 for comparison to zoning trends. The major similarity seems to be the coupled substitution $^{A}Ca^{Y}O \rightarrow {}^{A}Na^{Y}F$ (type 5, Aleshin and Roy, 1962). Differences include schemes involving vacancies; for example, $^{A}\square^{Y}\square \rightarrow {}^{A}Na^{Y}F$ is common in zoning patterns and $^{A}Ca^{Y}O \rightarrow {}^{A}\square^{Y}\square$ occurs as a result of alteration. These substitution schemes represent formation of Schottky-type defects during crystal growth and their filling during hydrothermal alteration. Both schemes fall under type 8 of Aleshin and Roy (1962). If Mn^{3+} enters the B site during alteration, then coupled substitutions like $^{A}Ca_2{}^{B}Mn \rightarrow {}^{A}Na_2{}^{B}Ta$ or $^{A}U^{6+B}Mn \rightarrow {}^{A}U^{4+B}Ta$ become plausible, the second scheme involving oxidation of U.

Chemical variations between lithologic units

The major-element chemistry, displayed in typical fashion on ternary diagrams for the A- and B-site cations (Figs. 3 and 4), does not allow the clear chemical distinction between microlites from different lithologic units. In order to determine if the microlites from different lithologic units are chemically distinct, the five groups of 217 microlite analyses were subjected to discriminant analysis on the basis of 20 variables consisting of the atomic compositions for all the elements determined and the sum of A-site cations. Discriminant analysis is a powerful tool for multivariant analysis (Davis, 1973) and classification improvement of complex mineral groups (e.g. Ewing, 1976). The purpose here is simply to describe the chemical differences among microlites from different lithologic units within the pegmatite and to identify the chemical changes due to primary hydrothermal alteration.

The discriminant analysis procedures used are those in the Statistical Analysis System software (SAS, 1982). One of several assumptions concerning the variables employed in multivariant procedures necessary to test the significance of differences between groups is that the variables have a multivariant normal

Table 5. Means and standard deviations of the most discriminating chemical variables by lithologic unit for the Harding pegmatite microlites

Variable	Quartz-lath spodumene zone	Cleavelandite unit	Microcline-spodumene zone	Lepidolite-cleavelandite subunit	Cleavelandite unit (in beryl zone)
U	0.02 ±0.01	0.06 ±0.06	0.14 ±0.05	0.13 ±0.03	0.07 ±0.04
Fe	0.001 ±0.002	0.01 ±0.01	0.004 ±0.007	0.03 ±0.02	0.03 ±0.02
Ti	0.01 ±0.01	0.02 ±0.02	0.04 ±0.03	0.04 ±0.03	0.09 ±0.07
Ca	1.09 ±0.07	1.02 ±0.09	1.09 ±0.15	1.03 ±0.14	1.07 ±0.05
Ce	0.004 ±0.003	0.006 ±0.001	0.003 ±0.003	0.005 ±0.001	0.004 ±0.003
Pb	0.001 ±0.002	0.009 ±0.01	0.01 ±0.02	0.005 ±0.001	0.01 ±0.009
F	0.70 ±0.09	0.65 ±0.17	0.43 ±0.13	0.51 ±0.06	0.57 ±0.14
Mn	0.008 ±0.09	0.01 ±0.02	0.05 ±0.04	0.02 ±0.01	0.03 ±0.02
Sb	0.005 ±0.002	0.006 ±0.003	0.005 ±0.003	0.006 ±0.002	0.008 ±0.004
Ta	1.77 ±0.06	1.74 ±0.07	1.65 ±0.07	1.63 ±0.04	1.63 ±0.15
Na	0.71 ±0.12	0.71 ±0.16	0.58 ±0.12	0.60 ±0.12	0.60 ±0.10
No. Cases	61	51	56	18	30

* Although the variables Bi, Ba and Th were significant, they are excluded because their values are near the minimum detection limit for the electron microprobe.

Table 6. Classification summaries for the groupings of lithologic units and *unaltered/altered,* using the set of most discriminating variables in each case

	Number of observations classified into:					
	A.	B.	C.	D.	E.	Totals
A. Quartz-lath spodumene zone	58	1	1	0	1	61
B. Cleavelandite unit	12	38	0	0	1	51
C. Microcline-spodumene zone	1	0	55	0	0	56
D. Lepidolite-cleavelandite subunit	0	0	0	18	0	18
E. Cleavelandite unit (in Beryl zone)	0	0	0	0	30	30
						216

	Number of observations classified into:		
	unaltered	altered	totals
unaltered	161	11	172
altered	4	40	44
			216

distribution. For the microlite data this is only approximately true, as many of the variables deviate from normality within groups by positive skewness. Fortunately, for mild deviations of this kind, the test statistics remain robust (Tabachnick and Fidell, 1983). We will not belabor the credibility of this and other assumptions (although they could be discussed at length), in that our goal is description rather than inference or classification.

As multivariant procedures can be adversely affected by outliers, the analyses were examined for outliers, and a single analysis with an unreasonably low total was removed. For the remaining 216 analyses, a stepwise discriminant procedure was applied to the groupings of lithologic units to determine the most significantly discriminating variables. Of the 20 variables examined, 14 were significant at the 2% level; they are (in order of decreasing F-value): U, Fe, Ti, Bi, Ca, Ce, Pb, F, Mn, Ba, Sb, Th, Ta, and Na (Table 5). However, the Bi, Ba, and Th values are near the minimum detection limit of the electron microprobe, so these are not meaningful. The classification summary in Table 6 allows the evaluation of the success of the discriminant analysis. In general, all of the microlite analyses are grouped correctly according to their a priori labels, except for those from the cleavelandite unit. A substantial number (23%) of those microlite analyses were misclassified into the quartz–lath spodumene zone. This indicates that the cleavelandite unit has chemical characteristics that overlap with those of the quartz–lath spodumene zone, which is not surprising, as the cleavelandite unit is, in part, a replacement of the quartz–lath spodumene zone. Because the overall groupings are correct, microlites from different lithologic units can be easily distinguished on the basis of their chemistry.

Linear combinations of the most discriminating variables were combined into four canonical variables, which are uncorrelated and have the highest possible multiple correlations with the lithologic units. Figure 10 displays a plot of the analyses and their group means for the first and second canonical variables. The first canonical variable provides the greatest separation between the quartz–lath spodumene zone and the microcline–spodumene zone, and these two lithologic units are in turn separated to the greatest extent by the second canonical variable from the lepidolite–cleavelandite subunit and the cleavelandite unit (in the beryl zone). This is most apparent in examining the positions of the group means in Figure 10. The maximum separation between groups occurs for the first and second canonical variables; however, Figure 10 is a projection in two dimensions of a four-dimensional (four canonical variables) plot. A certain amount of overlap in the projection is expected; however, much of the overlap for the quartz–lath spodumene zone and the cleavelandite unit persists even in four dimensions.

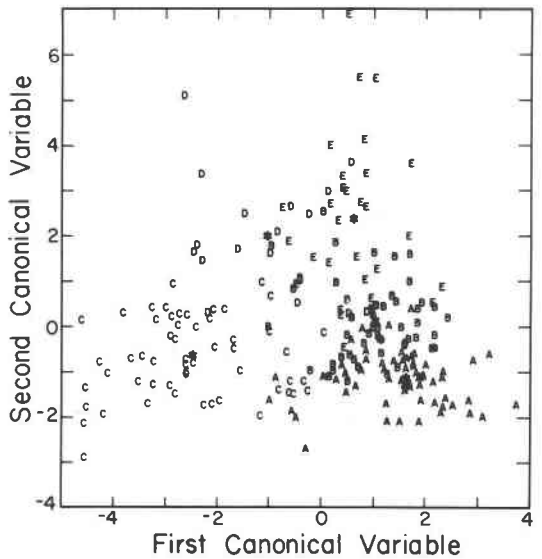

Fig. 10. Plot of the second versus the first canonical variable for the grouping by lithologic unit: quartz–lath spodumene zone (A), cleavelandite unit (B), microcline-spodumene zone, (C), lepidolite-cleavelandite subunit (D), and cleavelandite unit (in the beryl zone) (E). The asterisks mark the group means.

To follow the previous analysis using the groupings by lithologic unit, the 216 analyses were regrouped according to the labels *unaltered* and *altered,* which were determined primarily from SEM observations. The data base was not of sufficient size to divide the analyses within each lithologic unit. From the new grouping, the overall chemical changes ascribed to primary hydrothermal alteration can be identified. For the stepwise discriminant procedure, 5 of the 20 variables were significant at the 2% level, and they are (in order of decreasing F-value) Mn, Ti, Ca, Ba, and the A-site total (Table 7). The Mn, Ti, and Ca are higher in the altered samples, whereas the Ba and A-site totals are lower. The decrease in Ba, contrary to typical increases during alteration and weathering, cannot be ascribed any physical significance as the Ba values are nearly all at the minimum detection limits for the electron microprobe. Those microlites identified as being affected by hydrothermal alteration are restricted almost exclusively to the microcline-spodumene zone and cleavelandite unit (in the beryl zone). Consequently, increased Mn content in the altered samples may not be geochemically significant, because the microcline-spodumene zone microlites simply have the highest Mn contents. The increase of Ca and decrease of A-site cations is consistent with compositional changes established for alteration effects in AB_2O_6 Nb-Ta-Ti oxides (Ewing, 1975). The classification summary (Table 6) is grossly correct, but not as successful as for the lithologic units. Not surprisingly, alteration effects are less easily recognized than the lithologic unit containing the sample. Again, the single canonical variable in this case was constructed as a linear combination of the five discriminating variables. In Figure 11, the first canonical variable is plotted against Mn, to illustrate the separation between the two groups.

To examine the natural clustering of the microlite analyses without a priori labeling, disjoint cluster-analysis procedures were applied for cluster sizes ranging from two through six. For the cluster size of two, the groups correspond closely to those for the labels *altered/unaltered.* For the larger clusters, no natural groupings could be recognized other than those of lithologic unit.

Table 7. Means and standard deviations of the most discriminating chemical variables by the labels *unaltered/altered* for the Harding pegmatite microlites

variable	unaltered	altered
Mn	0.01 ±0.01	0.07 ±0.03
Ti	0.02 ±0.02	0.08 ±0.06
Ca	1.04 ±0.09	1.17 ±0.09
A-total	1.83 ±0.08	1.93 ±0.10
No. cases	172	44

* Although the variable Ba was significant, it was excluded because the values are near the minimum limit for the electron microprobe.

Chemical variations between lithologic units can be summarized as follows: (1) In primary units, the earliest microlites approach $NaCaTa_{1.8}Nb_{0.2}O_6F$ within the quartz–lath spodumene zone. (2) Subsequent crystallization of the microcline-spodumene core unit produced microlites with 0.4–0.7 Na, 0.1–0.2 U, 0.0–0.1 Pb, 0.2–0.4 Nb, 0.0–0.1 Ti, and 0.1–0.6 F atoms per formula unit. These are the highest U and lowest Na and F contents observed. Primary alteration produced up to 1.3 Ca and 0.1 Mn atoms per formula unit in microlites from this unit. (3) Microlites from the cleavelandite core unit are similar in composition to those of the quartz–lath spodumene zone except for 0.0–0.1 U and 0.4–0.8 F atoms per formula unit. (4) Where the cleavelandite unit replaced the beryl zone, microlites contain up to 0.03 Fe, 0.2 Ti, and 0.6 Nb atoms per formula unit. These are the highest values of Fe, Ti, and Nb observed in this study.

Radiation effects (metamictization)

Because of the wide variations in UO_3 content (less than 0.1 wt% to nearly 10 wt%), the microlites of the Harding pegmatite present a rare opportunity to study the effects of alpha-recoil damage on the pyrochlore structure-type as a function of increasing dose. These observations have important practical applications, as the pyrochlore structure-type is a common constituent of polyphase, crystalline, nuclear waste forms that have been proposed for the long-term isolation of actinides (Ringwood, 1982, 1985; Dosch et al., 1984; Morgan et al., 1984). Observations on the transition from the fully crystalline to X-ray diffraction amorphous state for the natural microlites over long periods of time (1300 m.y. B.P.) can be compared to synthetic pyrochlore structure-types that have been doped with ^{244}Cm or ^{238}Pu and observed to levels of equal dose (fully X-ray and electron diffraction amorphous) over periods of several years (Wald and Offermann, 1982; Clinard et al., 1984a, 1984b; Weber et al., 1985). We present here preliminary observations on the transition from the crystalline to metamict state for the Harding pegmatite microlites.

For each of the microlites analyzed, a total dose (alphas/mg) and the total number of displacements per atom (dpa) have been calculated. It is more common to calculate dose in units of alphas per cubic meter, but this requires a measured value for the density of each sample (the density decreases with increasing dose). The dose was calculated following the method of Holland and Gottfried (1955) based on the decay schemes for ^{238}U and ^{235}U. Because the Th concentration in the microlites is low, no consideration was given to alpha events associated with the decay of ^{232}Th. An age of 1300 m.y. B.P. was used (Brookins et al., 1979). With each alpha-decay event, a recoil nucleus (0.07 MeV) and an alpha particle (4 MeV) is produced. The range of the alpha particle is up to approximately 10 000 nm, but its energy is dissipated mainly by electronic excitation, ionization events, and at most several hundred atomic displacements. The recoil nucleus has a range of 10 nm, but because of its greater mass, it produces up to several thousand atomic displacements depending on the material. The number of displacements per atom is calculated assuming 1500 atomic displacements per alpha-decay event (Weber et al., 1982; Eyal and Fleischer, 1985). One must caution that in the correlation of changes in structural or physical properties with either dose or dpa for natural samples, "anomalous" samples may result from thermal events that have caused annealing and/or recrystallization. Alternatively, the calculated dose and dpa may be in error due to alteration that has removed or added U or Th to the sample. The special value of this extensive set of microlite data is that there are enough data available to clearly identify such "anomalous" samples.

The calculated doses for the Harding microlites range

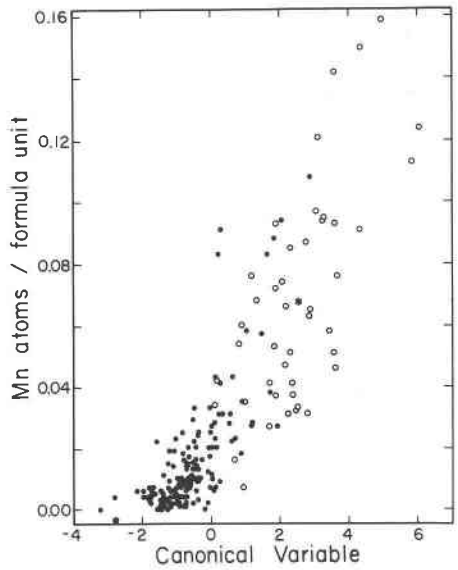

Fig. 11. Plot of the Mn content versus the canonical variable for the grouping by *unaltered* (solid circles) and *altered* (open circles). The asterisks mark the group means. For a single canonical variable, the data need only be plotted as a histogram; we chose to plot Mn because it is the most significantly discriminating variable.

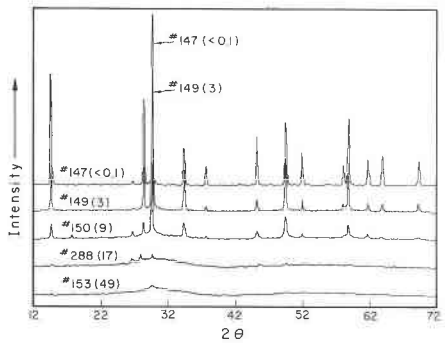

Fig. 12. Powder X-ray-diffraction scans for Harding pegmatite microlites. Numbers in parentheses are calculated values of the displacement/atom. Data for these samples are listed in Table 8.

Table 8. Summary of calculated doses (alphas/mg) and displacements per atom (dpa) for selected microlites from the Harding pegmatite

Sample No.	UO_3(wt.%)	alphas/mg	dpa	a_o^*
147	<0.05	$<10^{14}$	<1	10.429(1)*
149	0.8	3×10^{16}	3	10.428(1)
150	1.8	7×10^{16}	9	10.418(2)
288	3.2	1×10^{17}	17	10.389(4)
153	8.9	4×10^{17}	49	—

* Estimated standard errors (in parentheses) refer to the last digit.

from $<10^{14}$ to 4.5×10^{17} alphas/mg with equivalent dpa values of <0.1 to 61. The maximum doses are well beyond the doses normally required to cause a material to become X-ray or electron diffraction amorphous and well beyond doses commonly attained in doped materials. Experiments on doped, synthetic samples commonly reach doses of 10^{25} alphas/m^3, which is roughly equivalent to 10^{15} alphas/mg. It is interesting to consider the difference between the dose rate for the natural and synthetic samples. As an example, zirconolite (a pyrochlore structure-type derivative) doped with ^{238}Pu which has reached a dose of 10^{25} alphas/m^3 experiences a damage rate of 10^{-8} dpa/s (Clinard et al., 1984b). The microlites of the Harding pegmatite which have reached doses of 4×10^{17} alphas/mg have experienced a damage rate of 10^{-15} dpa/s, a rate fully seven orders of magnitude slower than that of the synthetic samples.

Selected X-ray powder diffractograms for unannealed microlites are illustrated in Figure 12, and the corresponding dose, displacement, and cell-parameter data for the samples are summarized in Table 8. The microlites retain good X-ray diffraction crystallinity up to doses of 10^{14} alphas/mg. In the range of 10^{16} alphas/mg there is a marked decrease in the intensity of the diffraction maxima, until at a dose of 10^{17} alphas/mg, there are no diffraction maxima. The decrease in X-ray intensity over a short range of the total dose is typical of the damage in-growth process and is seen in natural zircons (Holland and Gottfried, 1955), zircons doped with ^{238}Pu (Weber, pers. comm.), $Gd_2Ti_2O_7$ doped with ^{244}Cm (Wald and Offermann, 1982), and $CaZrTi_2O_7$ doped with ^{244}Cm and ^{238}Pu (Clinard et al., 1984a, 1984b). Although unit-cell refinements for the microlites having various levels of damage have been made (Table 8), there is no systematic evidence for the expansion of the unit cell with increasing damage as described for the synthetic samples in other studies. The observed decrease in a correlates with decreasing Na ($r_A = 0.118$ nm) and Ta ($r_B = 0.064$ nm) and increasing amounts of U^{4+} ($r_A = 0.100$ nm), U^{6+} ($r_A = 0.086$ nm), Ca ($r_A = 0.112$ nm), and Ti ($r_B = 0.061$ nm) in the five samples (Table 8). The microlite samples can be annealed by heating at 1000°C in air for 10 h. Although it is not possible to correlate the change in unit-cell volume directly with the degree of damage (owing to compositional variations), there is a slight decrease in the unit-cell volume for the annealed samples. Based on differential scanning calorimetry and differential thermal analysis, there is a dehydration endotherm at low temperature (150 to 300°C) and a recrystallization exotherm in the range of 450 to 600°C (Chakoumakos, 1978; Clinard, pers. comm.).

Details of the transition can be followed by the use of electron microscopy (Figs. 13, 14). The electron micrographs and their accompanying diffraction patterns show the atomic structure at doses of (a) 10^{14}, (b) 10^{16}, and (c) 10^{17} alphas/mg. At the intermediate dose (Fig. 14b), the lattice fringe image (two-beam image using the 111 reflection) shows that most of the microlite still retains its crystallinity, but with distinct patches or aggregates of aperiodic (no fringes) material. The electron-diffraction pattern is distinct, but with the added presence of a faint broad diffraction halo caused by the aperiodic areas. At the highest dose (Fig. 14c), there is no evidence for crystallinity, and we see only a multiple, broad-halo type diffraction pattern that is characteristic of an aperiodic structure. The equivalent d-spacing for the innermost halo is 0.298 nm. The interpretation of these electron-diffraction halos is discussed by Ewing and Headley (1983). Thus, the progression of structural modifications for natural microlites with increasing alpha dose is one of isolated defect aggregates (i.e., individual alpha-recoil tracks) up through doses of 10^{14} alphas/mg with no detectable effect on the material's ability to diffract X-rays or electrons, continued damage and overlap of these aggregates yielding coexisting regions of amorphous material and remaining crystalline domains in the range of 10^{15} to 10^{16} alphas/mg, with a final saturation value reached at $>10^{17}$ alphas/mg. A similar transition is observed over approximately the same range of doses for natural zirconolites and synthetic zirconolites that have been doped with ^{238}Pu (Ewing and Headley, 1983; Clinard et al., 1984a, 1984b). This suggests that there is no correlation between damage and dose rate even when the dose rate varies by as much as seven orders of magnitude. For the Harding pegmatite microlites, there is no evidence for significant annealing during the damage process.

The X-ray and electron-diffraction data do not allow one to explicitly describe the atomic structure of the final,

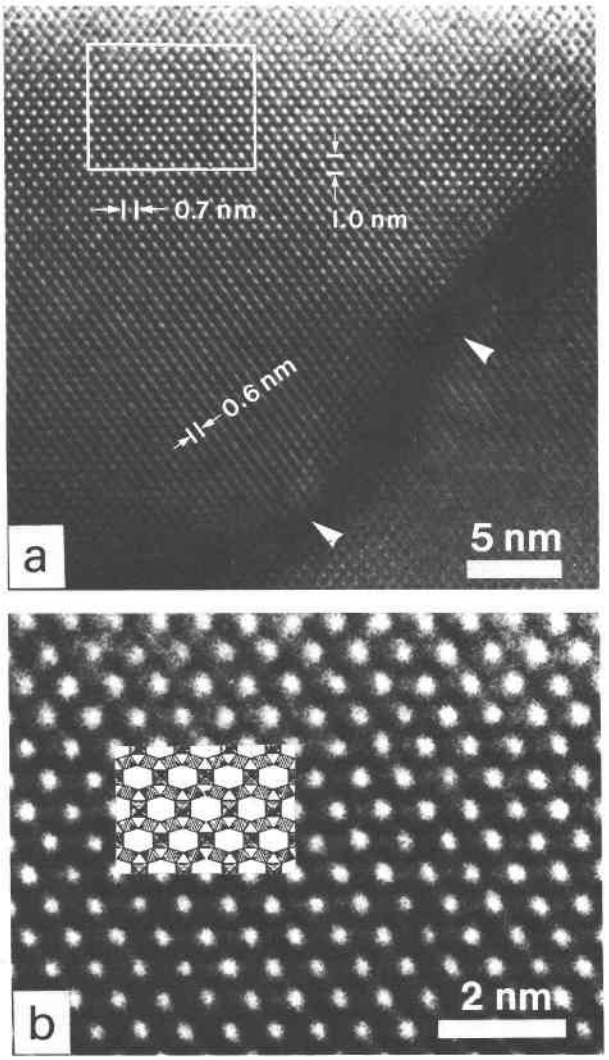

Fig. 13. Two-dimensional lattice image of crystalline microlite no. 147 in the (110) plane. (a) Principal lattice dimensions are given for the [001] (1.0 nm), [110] (0.7 nm), and [111] (0.6 nm) directions. Arrows denote dislocations within the band of lower contrast. (b) Enlarged region shown in (a) is interpreted in terms of the B_2O_6 framework structure of microlite.

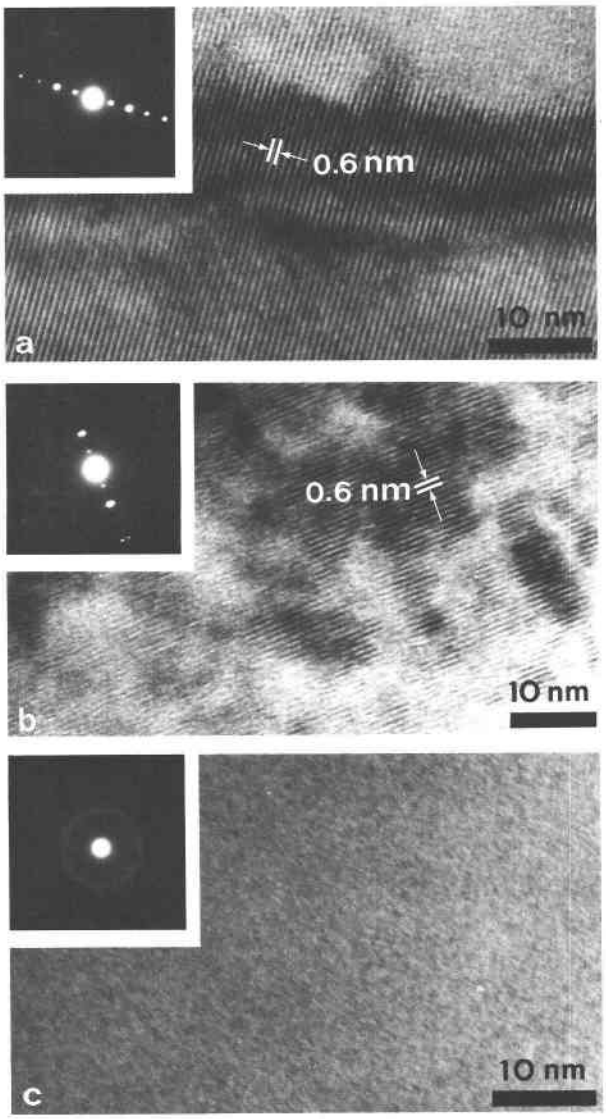

Fig. 14. Lattice-fringe images (two-beam image using the 111 reflection) and electron-diffraction patterns for microlites illustrating the effect of increasing alpha-event dose: (a) no. 147, (b) no. 150, and (c) no. 153. A summary of the data for each sample is given in Table 8.

damage-saturated state. It is important to understand the structure of this aperiodic state in order to evaluate whether further structural modifications may be expected with increasing dose. Structural information obtained from X-ray absorption spectroscopy for Ti and U (Greegor et al., 1985a, 1985b) indicates the persistence of TiO_6 octahedra and, tentatively, uranyl groups in metamict pyrochlore group minerals.

Summary and conclusions

Microlite, ranging from crystalline to metamict, is a principal accessory in several lithologic units of the Harding pegmatite, Taos County, New Mexico. From the sequence of lithologic units within the pegmatite, crystallization of microlite from the pegmatite magma is inferred to have begun relatively late, after the formation of the beryl and quartz zones, and continued throughout the formation of the core zones and subsolidus replacement units. Microlite is most abundant in the quartz–lath spodumene and microcline–spodumene ("spotted rock") zones. In both zones the microlite occurs as small subhedral to euhedral crystals commonly zoned from light cores to dark rims and never more than 5 mm in size.

Over 200 chemical analyses of microlite determined by electron microprobe are reported, and they are consistent with the accepted structural formula, $A_{2-m}B_2X_6Y_{1-n}O \cdot pH_2O$, where principally A = Ca, Na, U, Mn; B = Ta, Nb, Ti; X = O; and Y = F, OH, O. Typical ranges (weight percent) for major constituents are 60–78 Ta_2O_5, 2.5–12

Nb_2O_5, 0.0–3.2 TiO_2, 0.0–11 UO_2; 8.0–13 CaO, 2.0–5.5 Na_2O, 1.5–3.5 F, and 0.1–4.0 H_2O. Primary (hydrothermal) alteration results in an increase (in atoms per formula unit) in Mn of 0.05–0.10; Ca, 0.20–0.40; and O, 0.10–0.40. The H_2O content remains essentially constant. Secondary (weathering) alteration results in decreases (in atoms per formula unit) in Na of up to 0.7; Ca, 0.5; and F, 0.5. Low analytical totals in the probe results for altered areas suggest total H_2O contents of 8–13 wt%. The zoning in the individual crystals corresponds to three general types: (1) Nb, Na, and F decrease and Ta, Ca, U, Ti, and H_2O increase from core to rim; (2) cores are rich in Nb, Ta, Na, and F and rims are relatively rich in U, Ti, and H_2O; (3) Ta, Na, and F decrease and Nb, Ca, U, Ti, and H_2O increase from core to rim. The compositional variations between grains and the zoning relations are used to identify the principal substitution schemes in the microlite structure (Table 4). Major substitution schemes include (1) $^{A}Ca^{Y}O \rightarrow {}^{A}Na^{Y}F$ and (2) $^{A}\square^{Y}\square \rightarrow {}^{A}Na^{Y}F$ (zoning patterns) and (3) $^{A}Ca^{Y}O \rightarrow {}^{A}\square^{Y}\square$ (primary alteration). One of the most interesting correlations is the inverse relationship between U and F. On the basis of the assumption that the U is hexavalent, the data suggest that the uranium is in the cubic A site in the pyrochlore structure type with much the same coordination geometry as that found in the uranyl group. This is an important observation, as the uranyl group has been tentatively identified as a molecular unit in fully metamict pyrochlore group minerals (based on extended X-ray absorption fine-structure spectroscopy).

Multivariant analyses of the chemical variations in the microlites grouped according to lithologic unit demonstrate that unique chemistries characterize each group. Of 20 variables examined, 14 were significant at the 2% level; they are (in order of decreasing F-value): U, Fe, Ti, Bi, Ca, Ce, Pb, F, Mn, Ba, Sb, Th, Ta, and Na. In the single case of substantial misclassification (23% of the microlites in the cleavelandite unit were misclassified into the quartz–lath spodumene zone), the similarity is expected, as the cleavelandite unit is, in part, a replacement of the quartz–lath spodumene zone.

Radiation effects (metamictization) are clearly evident in the microlites. Because of the wide variations in UO_3 content (less than 0.1 wt% to nearly 10 wt%), the microlites exhibit the full range of structural periodicity from completely crystalline (<1 dpa), partially crystalline (up to 10–20 dpa), to completely X-ray and electron diffraction amorphous (>20 dpa). Based on X-ray and electron-diffraction analysis, the progressive structural modification of natural microlite with increasing alpha dose is one of isolated defect aggregates (i.e., individual alpha-recoil tracks) up through doses of 10^{14} alphas/mg with no effect on the material's ability to diffract X-rays or electrons, continued damage and overlap of these defect aggregates yielding coexisting regions of amorphous and crystalline domains at 10^{15} to 10^{16} alphas/mg, with a final saturation value received at doses greater than 10^{17} alphas/mg. The accumulated radiation damage postdates hydrothermal alteration and is contemporaneous and on-going with secondary (weathering) alteration.

Acknowledgments

Art Montgomery in donating the Harding pegmatite property to the University of New Mexico has preserved a unique outdoor geologic laboratory for research and teaching. His generous gift and continued support has stimulated renewed interest in this classic locality. R. C. Ewing is grateful for the many discussions he shared with Dick Jahns on the mineralogy and petrogenesis of the Harding pegmatite. Dick strongly supported the University of New Mexico's and Art Montgomery's efforts to preserve the Harding pegmatite as a classic locality for teaching and research. This paper only follows Dick's lead. We thank Eugene Foord, Lynn Boatner, Dick Jahns, and Paul Hlava for providing microprobe standards, Ian Mackinnon for assistance with the TEM, Elaine Faust-Stevens for drafting the figures, and Paula Stout for assistance with data and word processing. The authors are grateful for the thorough reviews by G. J. McCarthy and E. R. Vance.

The electron-microprobe analyses, scanning electron microscopy, and transmission electron microscopy were completed in the Electron Microbeam Analysis Facility in the Department of Geology and Institute of Meteoritics at the University of New Mexico supported in part by the Center for High Technology Materials.

This work was supported by the U.S. Department of Energy, Office of Basic Energy Sciences under grant #DE-FG04-84ER45099.

References

Aleshin, Eugene, and Roy, Rustum. (1962) Crystal chemistry of pyrochlore. American Ceramic Society Journal, 45, 18–25.

Aldrich, L.T., Wetherill, G.W., Davis, G.L., and Tilton, G.R. (1958) Radioactive ages of micas from granitic rocks by Rb-Sr and K-Ar methods. American Geophysical Union Transactions, 39, 1124–1134.

Bonshtedt-Kupletskaya, E.M. (1966) Systematization of the pyrochlore-microlite mineral group. Zapiski Vsesoinznoe Mineralogicheskoe Obshechestvo, 95, 134–144 (In Russian).

Borodin, L.S., and Nazarenko, I.I. (1957) Chemical composition of pyrochlore and diadochic substitution in the $A_2B_2X_7$ molecule. Geokhimiya, 4, 386–400 (transl. Geochemistry International, 4, 330–349, 1957).

Brookins, D.G., Chakoumakos, B.C., Cook, C.W., Ewing, R.C., Landis, G.P., and Register, M.E. (1979) The Harding pegmatite: Summary of recent research. In R.V. Ingersoll and L.A. Woodward, Eds. New Mexico Geological Society Guidebook, 30th Field Conference, Santa Fe Country, 127–133.

Černý, Petr. (1982) Anatomy and classification of granitic pegmatites. In P. Černý, Ed. Granitic pegmatites in science and industry, 1–40. Mineralogical Association of Canada Short Course Handbook 8.

Černý, Petr, and Burt, D.M. (1984) Paragenesis, crystallochemical characteristics, and geochemical evolution of micas in granitic pegmatites. In S.W. Bailey, Ed. Micas, 257–298. Mineralogical Society of America Reviews in Mineralogy, 13.

Chakoumakos, B.C. (1978) Microlite, the Harding pegmatite, Taos County, New Mexico. B.S. thesis, University of New Mexico, Albuquerque.

——— (1984) Systematics of the pyrochlore structure type, ideal $A_2B_2X_6Y$. Journal of Solid State Chemistry, 53, 120–129.

Chakoumakos, B.C., and Ewing, R.C. (1985) Crystal chemical constraints on the formation of actinide pyrochlores. In C.M. Jantzen, J.A. Stone, and R.C. Ewing, Eds. Scientific basis for nuclear waste management VIII, Materials Research Society Symposia, Proceedings, 44, 641–646. Materials Research Society, Pittsburgh.

Clinard, F.W., Jr., Rohr, D.L., and Roof, R.B. (1984a) Structural damage in a self-irradiated zirconolite-based ceramic. Nuclear Instruments and Methods in Physics Research, B1, 581–586.

Clinard, F.W., Jr., Peterson, D.E., Rohr, D.L., Hobbs, L.W. (1984b) Self-irradiation effects in ^{238}Pu-substituted zirconolite I. Temperature dependence of damage. Journal of Nuclear Materials, 126, 245–254.

Colby, J.W. (1968) MAGIC IV—A computer program for quantitative electron microprobe analysis. Advances in X-ray Analysis, 11, 287–305.

Davis, J.C. (1973) Statistics and data analysis in geology, chapter 7. Wiley, New York.

Dosch, R.G., Headley, T.J., and Hlava, Paul. (1984) Crystalline titanate ceramic nuclear waste forms: Processing and microstructures. American Ceramic Society Journal, 67, 354–361.

Ewing, R.C. (1975) Alteration of metamict, rare-earth, AB_2O_6-type Nb-Ta-Ti oxides. Geochimica et Cosmochimica Acta, 39, 521–530.

——— (1976) A numerical approach toward the classification of complex orthorhombic, rare-earth, AB_2O_6-type Nb-Ta-Ti oxides. Canadian Mineralogist, 14, 111–119.

Ewing, R.C., and Headley, T.J. (1983) Alpha-recoil damage in natural zirconolite ($CaZrTi_2O_7$). Journal of Nuclear Materials, 119, 102–109.

Eyal, Yehuda, and Fleischer, R.L. (1985) Preferential leaching and the age of radiation damage from alpha decay in minerals. Geochimica et Cosmochimica Acta, 49, 1155–1164.

Foord, E.E. (1976) Mineralogy and petrogenesis of layered pegmatite-aplite dikes in the Mesa Grande District, San Diego County, California. Ph.D. dissertation, Stanford University, Stanford, California.

——— (1982) Minerals of tin, titanium, niobium and tantalum in granitic pegmatites. In P. Černý, Ed. Granitic pegmatites in science and industry, 187–238. Mineralogical Association of Canada Short Course Handbook 8.

Greegor, R.B., Lytle, F.W., Chakoumakos, B.C., Lumpkin, G.R., and Ewing, R.C. (1985a) An investigation of metamict and annealed natural pyrochlores by X-ray absorption spectroscopy. In C.M. Jantzen, J.A. Stone, and R.C. Ewing, Eds. Scientific basis for nuclear waste management VIII, Materials Research Society Symposia Proceedings, 44, 655–662. Materials Research Society, Pittsburgh.

——— (1985b) An investigation of uranium L-edges of metamict and annealed pyrochlore. In L. Werme, Ed. Scientific basis for nuclear waste management IX, Materials Research Society, Pittsburgh, in press.

Harris, P.M. (1965) Pandaite from the Mrima Hill niobium deposit (Kenya). Mineralogical Magazine, 35, 277–290.

Heinrich, E.W., and Levinson, A.A. (1953) Studies in the mica group: Mineralogy of rose muscovites. American Mineralogist, 38, 25–49.

Hirschi, H. (1931) Mikrolith in Spodumenpegmatit bei Embudo in New Mexico. Schweizerische Mineralogische und Petrographische Mitteilungen, 253–255.

Hogarth, D.D. (1977) Classification and nomenclature of the pyrochlore group. American Mineralogist, 62, 403–410.

Holcombe, R.J., and Callender, J.F. (1982) Structural analysis and stratigraphic problems of Precambrian rocks of the Picuris Range, New Mexico. Geological Society of America Bulletin, 93, 138–149.

Holland, H.D., and Gottfried, David. (1955) The effect of nuclear radiation on the structure of zircon. Acta Crystallographica, 8, 291–300.

Jahns, R.H., and Ewing, R.C. (1976) The Harding mine, Taos County, New Mexico. In R.C. Ewing and B.S. Kues, Eds. New Mexico Geological Society, 27th Field Conference, Guidebook, 263–276.

——— (1977) The Harding mine, Taos County, New Mexico. Mineralogical Record, 8, 115–126.

Long, P.E. (1974) Contrasting types of Precambrian granitic rocks in the Dixon-Peñasco area, northern New Mexico. In C.S. Siemers, Ed. New Mexico Geological Society Guidebook, 25th Field Conference, Ghost Ranch (Central Northern New Mexico), 101–108.

Lumpkin, G.R., and Ewing, R.C. (1985) Natural pyrochlores: Analogues for actinide host phases in radioactive waste forms. In C.M. Jantzen, J.A. Stone, and R.C. Ewing, Eds. Scientific basis for nuclear waste management VIII, Materials Research Society Symposia Proceedings, 44, 647–654. Materials Research Society, Pittsburgh.

Mihálik, P.V.G. (1967) A chemical and mineralogical study of microlite from the Noumas pegmatite. M.S. thesis, University of the Witwatersrand.

Montgomery, Arthur. (1950) Geochemistry of tantalum in the Harding pegmatite, Taos County, New Mexico. American Mineralogist, 35, 853–866.

Morgan, P.E.D., Shaw, T.M., and Pugar, E.A. (1984) Ceramics for high waste loaded commercial radwaste disposal. In G.W. Wicks and W.A. Ross, Eds. Advances in ceramics, 8, 209–221. American Ceramic Society, Columbus, Ohio.

Norton, J.J. (1983) Sequence of mineral assemblages in differentiated granitic pegmatites. Economic Geology, 78, 854–874.

Pyatenko, Yu.A. (1959) Some aspects of the chemical crystallography of the pyrochlor-group minerals. Kristallografiya, 4, 204–208 (transl. Soviet Physics—Crystallography, 4, 184–186, 1960).

Ringwood, A.E. (1982) Immobilization of radioactive wastes in SYNROC. American Scientist, 70, 201–208.

——— (1985) Disposal of high-level nuclear wastes: A geological perspective. Mineralogical Magazine, 49, 159–176.

Saffiannikoff, A., and Van Wambeke, L. (1961) Sur un terme plombifere du groupe pyrochlore-microlite. Bulletin de la Société Française de Minéralogie et de Cristallographie, 84, 382–384.

SAS Institute, Inc. (1982) SAS user's guide: Statistics, 1982 edition. A.A. Ray, Ed. Cary, North Carolina.

Shannon, R.D. (1976) Revised effective ionic radii and systematic studies of interatomic distances in halides and chalcogenides. Acta Crystallographica, A32, 751–767.

Sitnin, A.A., and Bykova, A.V. (1962) The first specimen of microlite from granite. Doklady Akademii Nauk SSSR, 147, 203–206 (transl. Doklady Akademia Nauk SSSR, 147, 141–143, 1962).

Subramanian, M.A., Aravamudan, G., and Subba Rao, G.V. (1983) Oxide pyrochlores—A review. Progress in Solid State Chemistry, 15, 55–143.

Suchomel, T.J. (1976) Geology and mineralogy of the Harding pegmatite, Taos County, New Mexico. M.S. thesis, University of Illinois, Urbana-Champaign.

Tabachnick, B.G., and Fidell, L.S. (1983) Using multivariate statistics, chapter 9. Harper and Row, New York.

Van Wambeke, L. (1970) The alteration processes of the complex titano-niobo-tantalates and their consequences. Neues Jahrbuch für Mineralogie, 112, 117–149.

——— (1978) Kalipyrochlore, a new mineral of the pyrochlore group. American Mineralogist, 63, 528–530.

Von Knorring, Oleg, and Condliffe, Eric. (1984) On the occurrence of niobium-tantalum and other rare-element minerals in the Meldon aplite, Devonshire. Mineralogical Magazine, 48, 443–448.

Von Knorring, Oleg, and Fadipe, Akinola. (1981) On the mineralogy and geochemistry of niobium and tantalum in some granite pegmatites and alkali granites of Africa. Bulletin de la Société Française de Minéralogie et Cristallographie, 104, 496–507.

Wald, J.W., and Offermann, Peter. (1982) A study of radiation effects in curium-doped $Gd_2Ti_2O_7$ (pyrochlore) and $CaZrTi_2O_7$ (zirconolite). In W. Lutze, Ed. Scientific basis for nuclear waste management V, Materials Research Society Symposia Proceedings, 11, 369–378. North-Holland, New York.

Weber, W.J., Turcotte, R.P., and Roberts, F.P. (1982) Radiation

damage from alpha decay in ceramic nuclear waste forms. Radioactive Waste Management, 2, 295–319.
Weber, W.J., Wald, J.W., and Matzke Hj. (1985) Self-radiation damage in actinide host phases of nuclear waste forms. In C.M. Jantzen, J.A. Stone, and R.C. Ewing, Eds. Scientific basis for nuclear waste management VIII, Materials Research Society Symposia Proceedings, 44, 679–685. Materials Research Society, Pittsburgh.

Manuscript received May 2, 1985
Manuscript accepted November 4, 1985